

# Monte Carlo Integration with adaptive variance selection for improved stochastic Efficient Global Optimization

Felipe Carraro · Rafael Holdorf Lopez · Leandro Fleck Fadel Miguel ·  
André Jacomel Torii

the date of receipt and acceptance should be inserted later

**Abstract** In this paper, the minimization of computational cost on evaluating multi-dimensional integrals is explored. More specifically, a method based on an adaptive scheme for error variance selection in Monte Carlo integration (MCI) is presented. It uses a stochastic Efficient Global Optimization (sEGO) framework to guide the optimization search. The MCI is employed to approximate the integrals, because it provides the variance of the error in the integration. In the proposed approach, the variance of the integration error is included into a Stochastic Kriging framework by setting a target variance in the MCI. We show that the variance of the error of the MCI may be controlled by the designer and that its value strongly influences the computational cost and the exploration ability of the optimization process. Hence, we propose an adaptive scheme for automatic selection of the target variance during the sEGO search. The robustness and efficiency of the proposed adaptive approach were evaluated on global optimization stochastic benchmark functions as well as on a tuned mass damper design problem. The results showed that the proposed adaptive approach consistently outperformed the constant approach and a multi-start op-

timization method. Moreover, the use of MCI enabled the method application in problems with high number of stochastic dimensions. On the other hand, the main limitation of the method is inherited from sEGO coupled with the Kriging metamodel: the efficiency of the approach is reduced when the number of design variables increases.

**Keywords** stochastic kriging · efficient global optimization · integral minimization · adaptive target variance · robust optimization

## 1 Introduction

Much of today's engineering analysis consists of running complex computer codes. Although computer power has been steadily increasing, the expense of running many analysis codes remain non-trivial. For example, a single evaluation of a finite element model may take minutes to hours, if not longer. Thus, it often becomes impractical to perform a large number of such simulations, for example, as required during optimization. To address such a challenge, approximation or metamodeling techniques are often used.

One of such techniques is Kriging (Krige, 1951; Cressie, 1993), which has been gaining popularity in the last decade, and has been applied in numerous branches of science (Theodossiou and Latinopoulos, 2006; Goel et al., 2008; Huang et al., 2011; Sakata et al., 2011; Zhu et al., 2014). It has been shown to produce accurate response surfaces and to offer a estimate of the error in points that had not been sampled.

Kriging in its usual formulation considers the approximation of deterministic functions. But what if the objective function possess some sort of randomness or

Felipe Carraro, E-mail: felipecarraro@gmail.com  
Rafael Holdorf Lopez, E-mail: rafael.holdorf@ufsc.br  
Leandro Fleck Fadel Miguel, E-mail: leandro.miguel@ufsc.br

Center for Optimization and Reliability in Engineering (CORE), Civil Engineering Department, Federal University of Santa Catarina, Rua João Pio Duarte Silva, s/n 88040-900 Florianópolis, SC, Brazil.

André Jacomel Torii, E-mail: ajtorii@hotmail.com

Center for Optimization and Reliability in Engineering (CORE), Civil Engineering Department, Federal University for Latin American Integration, Av. Silvio Américo Sasdelli, 1842 - Vila A, 85866-000 Foz do Iguaçu, PR, Brazil

variability? This randomness could be, for example, uncertainty in the input parameters or noise in the function response. For such cases, a more recent extension called Stochastic Kriging (SK) (Staum, 2009; Ankenman et al., 2010; Kleijnen and Mehdad, 2016; Kamiński, 2015; Chen and Kim, 2014; Plumlee and Tuo, 2014) was developed. Improvements and extensions emerged for both SK and deterministic Kriging in recent years. For example, Wang et al. (2014) included qualitative factors on the SK metamodel by constructing correlation functions that are valid across levels of qualitative factors. Several authors incorporated gradient estimators into the metamodel, which tends to significantly improve surface prediction (Chen et al., 2013; Qu and Fu, 2014; Ulaganathan et al., 2014; Hao et al., 2018). Chen and Kim (2014) evaluated sampling strategies while taking into account possible bias in SK simulation response estimates. Plumlee and Tuo (2014) suggested an approach where the intrinsic metamodel of SK error is not assumed Gaussian distributed, deriving a distributional emulator called Quantile Kriging. In the same subject, Zhang and Xie (2017) built the Asymmetric Kriging emulator, again without error distribution assumption. This approach employed asymmetric least squares, which are used to compute multiple quantile curves and fit the model. Kamiński (2015) proposed an improved SK update procedure by combining metamodel and simulation evaluations in addition to the use of smoothed variance evaluations to compute the intrinsic noise. Shen et al. (2018) applied stylized queuing models to provide information about the shape of the response surface. Following Chen et al. (2012), Zou and Zhang (2018) further explored the use of Common Random Numbers with SK, showing that its use may not always be detrimental to prediction accuracy, being beneficial if the observation errors of the real system are small enough.

A powerful approach to use Kriging or SK within an optimization context is the Efficient Global Optimization (EGO). EGO is the name of the framework developed by Jones et al. (1998), which exploits the information provided by the Kriging metamodel to iteratively add new points, improving the surrogate accuracy and at the same time seeking its global minimum. It is the manner in which these infill points are added that characterizes different EGO methods.

The use of SK within the EGO framework, which we name here stochastic Efficient Global Optimization (sEGO), is relatively recent. For example, Jalali et al. (2017) compared Kriging-based methods in heterogeneous noise situations, while Picheny et al. (2013b) benchmarked different infill criteria for the noisy case. The choice of infill in stochastic environment has received

considerable attention in literature. Some authors considered the use of the classical (noiseless) Expected Improvement (EI) criterion with a “plug-in”, which is effectively an target for the definition of improvement, such as Vazquez et al. (2008) and Osborne et al. (2009). Unfortunately, for the noisy case plug-ins do not take into account the noise of future observations. The Augmented Expected Improvement (AEI) method from Huang et al. (2006), addresses this issue with a penalty term. Such formulation is employed in this paper and is further discussed in subsection 3.3. Forrester et al. (2008) employed a reinterpolation procedure by building one model for evaluating and predicting noisy observations and another interpolative model for determining the infill point. Picheny et al. (2013a) considered a modification of EI using quantiles to define a reference for improvement, taking into account the effect of a new observation on the model. The work of Scott et al. (2011) applied the concept of knowledge gradient to define improvement, aiming to measure the global effect of a new measurement on the model mean. Methods employing a global measure of improvement have also been proposed, however those involve potentially expensive numerical integrations. Villemonteix et al. (2009) criterion maximized information gain, while Gramacy and Lee (2010) evaluated the effect of a candidate point over the design space with an Integrated Expected Conditional Improvement.

In this context, this paper presents an efficient sEGO approach for optimization problems whose objective function depends on an integral. The proposed approach is based on Monte Carlo Integration (MCI) and sEGO. First, MCI is employed to approximate the objective function since it provides not only an approximation for the integral, but also the variance of the error. The variance of the error is then included into the SK framework, and the AEI infill criterion is employed to guide the addition of new points in the stochastic EGO framework. We show that the variance of the error committed by MCI may be controlled by the designer and that its value strongly influences the computational cost and the exploration ability of the optimization process. Thus, the main contribution of this paper is the development of an adaptive scheme for the evaluation of a target variance of the error committed by MCI. The adaptive approach provides a framework to avoid getting stuck in local minima due to lack of information, and to achieve an efficient optimization process by rationally spending the available computational budget, *i.e.* it balances the exploration and exploitation capabilities of the algorithm.

The rest of the paper is organized as follows: section 2 presents the problem statement, *i.e.* the charac-

teristics of the problems we aim to solve as well as a description of the MCI. The sEGO framework is presented in section 3. The potential consequences of the target variance setting are detailed in section 4, while the adaptive target approach is presented in section 5. Numerical examples are studied in section 6 to show the efficiency and robustness of the proposed method. Finally, the main conclusion are listed in section 7.

## 2 Problem Statement

The goal of this paper is to solve the problem of minimization of a function  $J$ , which depends on an integral as in

$$\min_{\mathbf{d} \in S} J(\mathbf{d}) = \int_{\Omega} \phi(\mathbf{d}, \mathbf{x}) w(\mathbf{x}) d\mathbf{x}, \quad (1)$$

where  $\mathbf{d} \in \mathbb{R}^n$  is the design vector,  $\mathbf{x} \in \mathbb{R}^{n_x}$  is the parameter vector,  $\phi : \mathbb{R}^n \times \mathbb{R}^{n_x} \rightarrow \mathbb{R}$  is a known function,  $S$  is the design domain,  $w(\mathbf{x})$  is some known weight function (*e.g.* probability distribution) and  $\Omega \subseteq \mathbb{R}^{n_x}$  is the integration domain (*e.g.* support of the probability distribution). We also assume here that the design domain  $S$  considers only box constraints.

Here we are interested in situations that:

- this integral cannot be evaluated analytically,
- $\phi$  is a black box function and is computationally demanding,
- the resulting objective function  $J$  is not convex and multimodal,
- $S$  includes only box constraints.

To give only a few examples, in engineering applications problems of this kind may arise from the maximization of the expected performance of a mechanical system, vastly applied in robust design (Capiez-Lernout and Soize, 2008; Soize et al., 2008; Ritto et al., 2011; Lopez et al., 2014; Fadel et al., 2016; Miguel et al., 2016), the multidimensional integral of Performance Based Design Optimization (Beck et al., 2014; Spence and Kareem, 2014; Bobby et al., 2016), or the double integral of Optimal Design of Experiment problems (Huan and Marzouk, 2013; Beck et al., 2018).

In the formulation of Eq. (1), it is important to notice the difference between  $n$ , which is the dimension of the optimization problem and  $n_x$ , which is the stochastic dimension of the integral. Indeed, in cases where the integration domain  $\Omega$  of Eq. (1) has high dimension, evaluation of the above integral may become computationally demanding. Numerical integration such as quadrature procedures may be employed,

although its computational efficiency is drastically reduced for high dimensional problems. In such cases, together with the sEGO approach proposed in this paper, sampling techniques may be employed, such as MCI, Importance Sampling (Rubinstein, 2007), Multi Level Monte Carlo (Giles, 2008), Multi index Monte Carlo (Haji-Ali et al., 2016).

In MCI,  $J$  is estimated as

$$J(\mathbf{d}) \approx \bar{J}(\mathbf{d}) = \frac{1}{n_r} \sum_{i=1}^{n_r} \phi(\mathbf{d}, \mathbf{x}^{(i)}), \quad (2)$$

where  $n_r$  is the sample size and  $\mathbf{x}^{(i)}$  are sample points randomly drawn from distribution  $w(\mathbf{x})$ . In this work the sample points employed for MCI are also called replications, in order to distinguish from sample points employed for Kriging, when necessary.

One of the advantages of using sampling techniques, such as MCI, is that we are able to estimate the variance of the error of the approximation. Indeed, the variance of the estimator can be computed for a fixed  $\mathbf{d}$  by a point estimate as:

$$\bar{\sigma}^2(\mathbf{d}) = \frac{1}{n_r(n_r - 1)} \sum_{i=1}^{n_r} (\phi_i - \bar{J}(\mathbf{d}))^2, \quad (3)$$

where  $\phi_i = \phi(\mathbf{d}, \mathbf{x}^{(i)})$ . Thus, by increasing the sample size  $n_r$  (*i.e.* the number of replications), the variance estimate decreases and approximation in Eq. (2) gets closer to the exact value of Eq. (1). In fact, it may be demonstrated that the rate of convergence of MCI is  $n_r^{-\frac{1}{2}}$  (Hammersley and Handscomb, 1964; Kalos and Whitlock, 1986).

As already mentioned, in this paper we aim to solve problems in which  $\phi$  is a black box computationally demanding function, and  $J$  is nonconvex. We assume gradient information is unknown, although such information, if available, could be employed as in Hao et al. (2018). EGO algorithms are able to handle these difficulties and were successfully applied in different fields (Couckuyt et al., 2010; Li and Heap, 2011; Bae et al., 2012; Duvigneau and Chandrashekar, 2012; Gengembre et al., 2012; Kanazaki et al., 2015; Chaudhuri et al., 2015; Haftka et al., 2016; Ur Rehman and Langelaar, 2017). More specifically, in this paper we propose the use of sEGO, but the SK metamodel is enriched with the information given by Eq. (3). EGO, SK and the proposed scheme are detailed in the next sections.

### 3 Stochastic Efficient Global Optimization (sEGO)

According to Jones (2001), EGO methods generally follow these steps:

1. Construction of the initial sampling plan;
2. Construction of the metamodel;
3. Addition of a new infill point to the sampling plan and return to step 2.

Steps 2 and 3 are repeated until a stop criterion is met, *e.g.*, maximum number of function evaluations. The manner in which the infill points are added in each iteration is what differs the different EGO approaches. In the next subsections, these steps are detailed in order to set the basis of the proposed approach.

#### 3.1 Initial sampling plan

In the first step, a Kriging sampling plan  $\Gamma$  containing  $n_s$  points is created, *i.e.*

$$\Gamma = \{\mathbf{d}^{(1)}, \mathbf{d}^{(2)}, \dots, \mathbf{d}^{(n_s)}\}. \quad (4)$$

A Latin Hypercube scheme is usually employed for this purpose. Then, the objective function value  $J$  of each of these points is evaluated using the original model, obtaining

$$\mathbf{y} = \{y^{(1)}, y^{(2)}, \dots, y^{(n_s)}\}, \quad (5)$$

where  $y^{(i)} = J(\mathbf{d}^{(i)})$ .

Step 2 constructs a prediction model, which is given by the SK in this paper. In order to keep the paper self-contained, the formulation of Deterministic Kriging is given in Appendix A, while the SK formulation is given in the next subsection.

#### 3.2 Stochastic Kriging (SK)

Ankenman et al. (2010) proposed an extension to the deterministic Kriging methodology to deal with stochastic simulation. Their main contribution was to account for the sampling variability that is inherent to a stochastic simulation. In order to accomplish this, they characterized both the intrinsic error inherent in a stochastic simulation and the extrinsic error that comes from the metamodel approximation. Then, the SK prediction can be seen as:

$$\hat{y}(\mathbf{d}_i) = \overbrace{M(\mathbf{d}_i)}^{\text{Trend}} + \overbrace{Z(\mathbf{d}_i)}^{\text{Extrinsic}} + \overbrace{\epsilon(\mathbf{d}_i)}^{\text{Intrinsic}}, \quad (6)$$

where  $M(\mathbf{d})$  is the usual average trend,  $Z(\mathbf{d})$  accounts for the model uncertainty and is now referred as extrinsic noise. The additional term  $\epsilon$ , called intrinsic noise, accounts for the simulation uncertainty or variability. In the original version of Ankenman et al. (2010), the intrinsic noise is assumed independent and identically distributed (i.i.d.) across Kriging sample points and possess a Gaussian distribution with zero mean.

In the present paper, the variability is due to the error in the approximation of the integral from Eq. (1) caused by MCI. It is worth to recall here that MCI provides an estimation of the variance of this error. That is, we are able to estimate the intrinsic noise, and consequently, introduce this information into the metamodel framework. In order to accomplish this, we construct the covariance matrix of the intrinsic noise - among the current sampling plan points. Since the intrinsic error is assumed to be i.i.d. and Normal, the covariance matrix is a diagonal matrix with components

$$(\Sigma_\epsilon)_{ii} = \bar{\sigma}^2(\mathbf{d}_i), \quad i = 1, 2, \dots, n_s, \quad (7)$$

where  $\bar{\sigma}^2$  is given by Eq. (3). Then, considering the Best Linear Unbiased Predictor shown by Ankenman et al. (2010), the prediction of the SK at a given point  $\mathbf{d}_u$  is:

$$\hat{y}(\mathbf{d}_u) = \hat{\mu} + \mathbf{r}^T(\Psi + \Sigma_\epsilon)^{-1}(\mathbf{y} - \mathbf{1}\hat{\mu}), \quad (8)$$

which is the usual Kriging prediction with the added diagonal correlation matrix from the intrinsic noise, as can be seen by comparing Eqs. (8) and (42).

Similarly, the predicted error takes the form:

$$s_n^2(\mathbf{d}) = \widehat{\sigma}^2 \left[ 1 + \lambda(\mathbf{d}) - \mathbf{r}^T(\Psi + \Sigma_\epsilon)^{-1}\mathbf{r} + \frac{(1 - \mathbf{1}^T(\Psi + \Sigma_\epsilon)^{-1}\mathbf{r})^2}{\mathbf{1}^T(\Psi + \Sigma_\epsilon)^{-1}\mathbf{1}} \right], \quad (9)$$

where  $\lambda(\mathbf{d})$  corresponds to the regression term. If the errors are assumed homoscedastic, then this term becomes a constant and  $\Sigma_\epsilon = I\lambda$ . In the present paper, the designer may set its value in the MCI, *i.e.* its value depend on the selected variance  $\bar{\sigma}^2$ . Further discussion on the how targets are chosen is presented in section 4.

### 3.3 Infill criterion for stochastic EGO

Although SK provides a good noise filtering model, the error estimates are no longer appropriate for use when choosing infill points in the EGO framework (J. Forrester et al., 2006).

The popular Expected Improvement (EI) infill criteria has proven global convergence under the deterministic case (Locatelli, 1997). However, this property no longer holds for the stochastic case, which does not guarantee a dense sampling. Overall, any method that relies on the predicted error going to zero at sampled points, which is the case in the deterministic approach, has difficulties for application in stochastic environments (J. Forrester et al., 2006). Hence, an infill point method adapted to SK is required. Picheny et al. (2013b) benchmarked different infill criteria for SK case. From that paper, a modification of the deterministic EI criterion called AEI (Huang et al., 2006) provided promising results and it is employed here. The main steps of the AEI criterion are presented in the next paragraphs, while a full description is given by Huang et al. (2006) and Picheny et al. (2013b). Moreover, comparison of AEI to deterministic infill criteria may be found in references Huang et al. (2006); Forrester et al. (2008).

In the EI criterion, the infill point is selected as the one that maximizes the expected value of the improvement measurement. This improvement definition requires a target value to indicate the greediness of the search. Considering the improvement definition:

$$I(\mathbf{d}, y_{\text{target}}) := \max(0, y_{\text{target}} - Y(\mathbf{d})), \quad (10)$$

where the  $y_{\text{target}}$  for EI is usually chosen as the minimal solution found so far. For the AEI infill criterion, this target is the so-called effective best solution  $\mathbf{d}^{**}$  and is computed as:

$$\mathbf{d}^{**} = \underset{i}{\operatorname{argmin}}(\mathbf{d}^{(i)} + \alpha s_n^{(i)}) \quad \text{for } i = 1, \dots, n_s, \quad (11)$$

where  $s_n^{(i)}$  is the corresponding kriging error, obtained by taking the square root of the MSE defined in Eq. (9), and  $\alpha$  is an arbitrary constant.

The criterion can be calculated as the expected improvement over the effective best solution multiplied by a penalization term:

$$AEI(\mathbf{d}) = \mathbb{E}[I(\mathbf{d}, \mathbf{d}^{**})] \left( 1 - \frac{\sqrt{\lambda(\mathbf{d})}}{\sqrt{s_n^2(\mathbf{d}) + \lambda(\mathbf{d})}} \right), \quad (12)$$

where  $\mathbb{E}[I(\mathbf{d}, \mathbf{d}^{**})]$  represents the expected value of the already defined improvement,  $s_n^2$  the Kriging estimated error and  $\lambda$  the intrinsic output noise, which will be enforced by MCI procedure based on a target variance.

The term between parenthesis in the right-hand-side of Eq. (12) is a penalty factor which amplifies the importance of the Kriging variance. That is, it enhances exploration, avoiding multiple simulations over the same input (Picheny and Ginsbourger, 2014).

### 4 Problem: how to set the target variance?

With the framework presented so far, we are able to incorporate error estimates from MCI within the sEGO scheme. It is important to notice that the number of samples (replications) of the MCI is an input parameter, *i.e.* the designer has to set  $n_r$  in Eq. (3). Consequently, the designer is able to control the magnitude of  $\Sigma_\epsilon$  and  $\lambda$  by changing the sample size  $n_r$ . However, in practice a target variance ( $\bar{\sigma}_{\text{target}}^2$ ) is first chosen and the sample size is iteratively increased until the evaluated variance is close to the target value. Thus, for a constant target variance, the regression parameter is then enforced by the MCI procedure to be

$$\lambda(\mathbf{d}) = \bar{\sigma}_{\text{target}}^2. \quad (13)$$

The choice of the target variance must consider two facts:

- if the target variance is too high, the associated error may lead to a poor and deceiving approximation of the integral,
- if the target tends to zero, so does the error and we retrieve the deterministic case, however, at the expense of a huge computational effort.

This section aims to emphasize the importance of the target variance setting and its consequences in the optimization process using stochastic EGO. It presents the key ideas behind the main contribution of this paper: the adaptive target variance approach proposed in Section 5.

In order to better visualize the optimization procedure, consider the following multimodal function:

$$\phi(d, X) = -(1.4 - 3d) \sin(18d)X, \quad (14)$$

where  $X$  is a Normal random variable with mean 1 and standard deviation 0.1 (*i.e.*  $X \sim \mathcal{N}(1, 0.1)$ ). Here, we want to find  $d^*$  that minimizes the expected value of

this function in the design domain  $d \in S = [0, 1.2]$ . That is, our problems resumes to:

$$\min_{d \in S} J(d) = \mathbb{E}[\phi(d, X)] = \int_{\Omega} \phi(d, x) f_X(x) dx, \quad (15)$$

where  $\mathbb{E}$  is the expected value operator,  $f_X$  is the Normal probability density function of  $X$  and  $\Omega = (-\infty, +\infty)$  its support. Figure 1 illustrates the approximation of  $J$  given by MCI over the design domain, *i.e.* it plots  $\bar{J}$ , evaluated using Eq. (2), over the design domain.

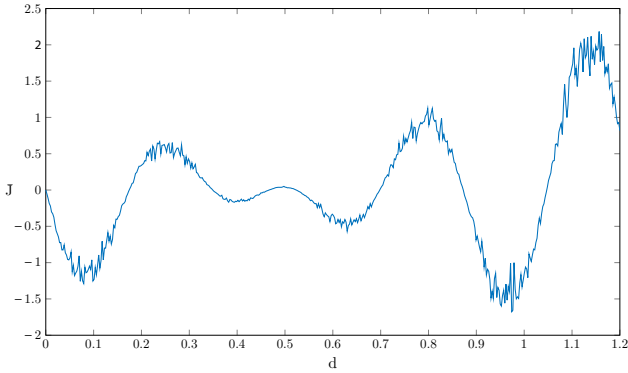


**Fig. 1** Approximation of  $J$  given by MCI

As described in section 3, the first step of an EGO algorithm is the construction of the initial sample plan. Here, we employ the initial Kriging sample size as  $n_s = 5$ , which may be visualized as the blue dots in Figs. 2a or 2b. Each observation is replicated  $n_r$  times in order to achieve the desired target variance ( $\bar{\sigma}_{target}^2$ ).

As already mentioned, different targets imply different error estimates, *i.e.* the more replications we draw at a given design vector, the lower is the variability of the MCI estimate. For example, Figure 2a shows a SK model based on  $\bar{\sigma}_{target}^2 = 1.00$ , while Figure 2b shows the model resulting from the same initial Kriging sample, but in this case with  $\bar{\sigma}_{target}^2 = 0.001$ . In these figures, the dashed red lines represent the SK model prediction, given by Eq. (8), while the dashed gray lines give the variability of the SK model, which correspond to the interval  $[-s_n, +s_n]$  from the prediction, which is evaluated by Eq. (9).

In deterministic Kriging, the estimated error is exactly zero at sampled points. However, when  $J$  is estimated using MCI, the error only approaches zero as the number of replications increases (*i.e.* when  $n_r \rightarrow \infty$ ). For instance, comparing both cases in Fig. 2, it can be seen that the RMSE interval is closer to the sampled points in Figure 2b while it is quite far in Figure 2a. Although a larger number of evaluations is needed in order to achieve a lower target variance, it can be seen that

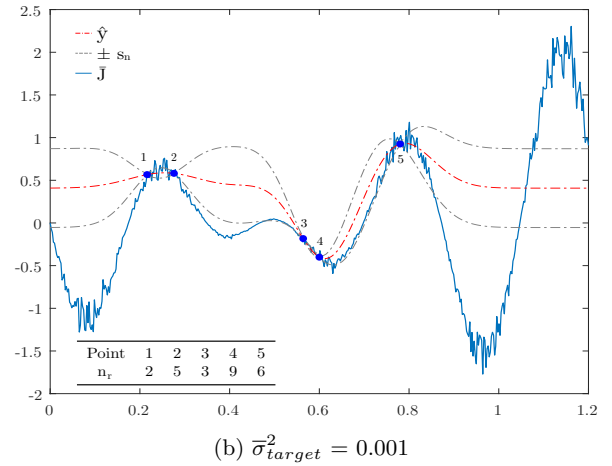
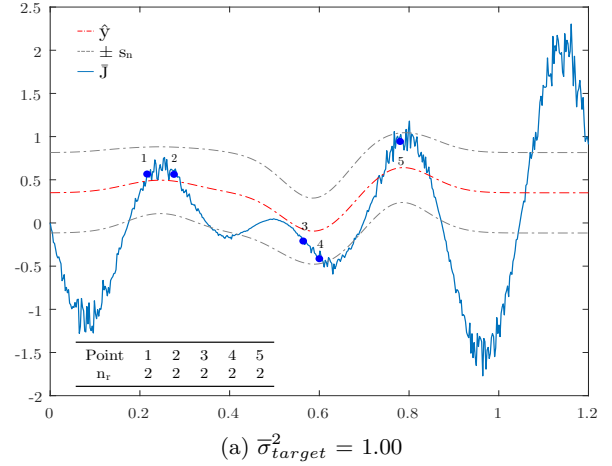


**Fig. 2** Different model based on the estimated error

it may improve the prediction. Having a more accurate description of the function with a lower estimated error on sampled points makes the infill criterion approach the deterministic case, which is known to be globally convergent.

After the initial SK model construction, the next step in the EGO procedure is the refinement of the model by adding infill points. Using the AEI criterion, the point that minimizes the utility function composed of an EI term and a penalty term is added to the model (see Eq. (12)).

Consider first the case in which we have a relatively low target variance, *i.e.*  $\bar{\sigma}_{target}^2 = 0.01$ . Figure 3 illustrates how the AEI infill works. The auxiliary plot presented below the function plot represents the negative of the AEI measure over the domain. The circled point indicates the selected infill point, which is shown to maximize the AEI measure (*i.e.* it minimizes  $-AEI$ ).

Figure 4 shows the progress of the optimization in two different moments. In Fig. 4a, the 5th infill is added to the model. The search has not found the optimal

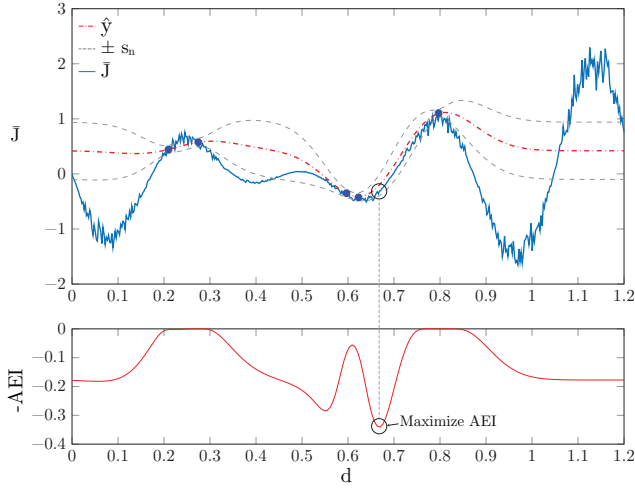


**Fig. 3** AEI plot over the domain

valley yet. The search proceeds and after some evaluations on the initial valley the algorithm starts exploring more uncertain regions. By the 20th infill, it is possible to see in Fig. 4b that the algorithm already sampled around the global optimum multiple times. Therefore, AEI value is very low and directed to that single region.

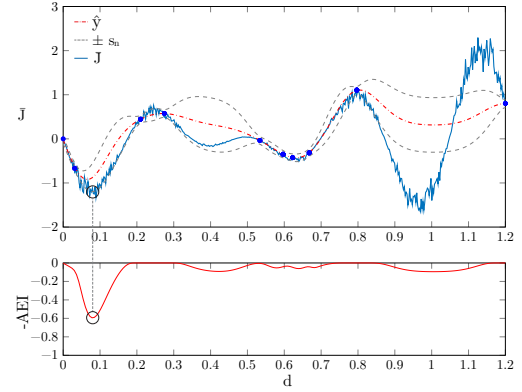
A completely different situation occurs when we consider the case in which we have a relatively high target variance, *i.e.*  $\bar{\sigma}_{target}^2 = 1.00$ . As it may be seen in Fig. 5, which shows the search at the 30<sup>th</sup> infill point, the optimization process stalls at the first valley found and never explores other regions. This is caused by the lack of information gained by each point added to the model. Each infill is inserted considering the unit target variance. Because the estimated error remains almost the same, the infill criterion becomes highly local, avoiding exploration of potentially better regions. The penalization from AEI only takes effect when  $s_n^2$  is low, which is not the case when the target variance is high.

The main conclusion from this section is that there is a need for a rational adaptive choice of the target variance. A higher target reduces computational cost, yet it can become highly local. A lower target may need higher computational cost, however the refined model is more easily exploited. A trade-off between these characteristics must be made in order to:

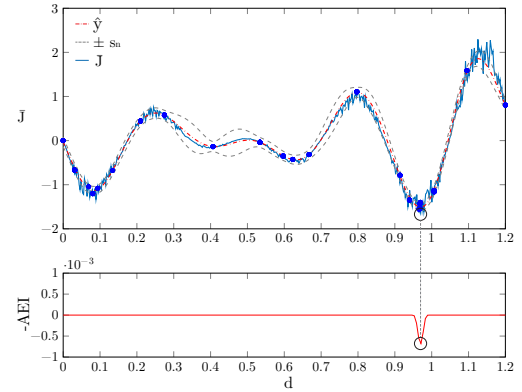
- avoid getting stuck in local minima due to lack of information,
- achieve an efficient optimization process.

## 5 Proposed approach: adaptive target selection

As it was seen in the previous section, the target variance plays an important role when using the MCI



(a) Infill 5



(b) Infill 20

**Fig. 4** Refinement of the SK model seeking the optimal value with target variance 0.01.

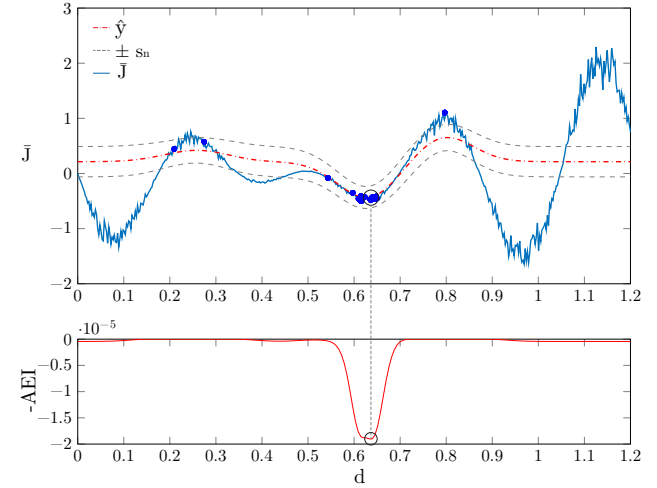


**Fig. 5** Stalling at infill 20 with target variance 1.00.

coupled with SK. Setting it either too small or too high may hinder the optimization algorithm. When too small, the target forces a large number of evaluations on a single point, effectively compromising the computational budget of the global optimum search. On the other hand, setting it too high may stall the search due to the lack of reliable information obtained with each infill, as shown in Fig. 5.

As it can be inferred, the efficiency and the success of the optimization approach depends on the target selected. However, which target to choose? The main contribution of this paper is proposing an adaptive target selection procedure. This idea arises to confront the existing drawbacks of both low and high targets, as discussed in section 4. However, instead of a simple middle ground constant target variance value, here we suggest a more efficient approach.

The proposed approach consists on an adaptive target selection. It aims to balance the trade-off between accuracy and computational cost. The main idea is similar to an exploration versus exploitation aspect of any global optimization procedure. The adaptive approach starts exploring the design domain by evaluating the objective function value of each design point using MCI with a high target variance - so that each evaluation requires only a few samples. That is, the initial target value  $\bar{\sigma}_{target}^2$  should be initially set to a value that avoids expending too much computational resources at the first iterations of the algorithm, giving room for the adaptive scheme to work.

Then, it gradually reduces the target variance for the evaluation of additional infill points in regions of the design domain where points were already sampled. It is expected that such a reduction make the algorithm exploit the promising regions of the design domain, not stalling the search as the example of section 4.

A flowchart of the proposed stochastic EGO algorithm, including the proposed adaptive target selection, is shown in Fig. 6. In the next paragraphs, each of its steps is detailed.

The first step is the creation of the Kriging sampling plan. Here, we employed the Latin Hypercube method presented in Forrester et al. (2008). It is important to highlight here that all design points of the sampling plan are evaluated using  $n_r = 1$ , ignoring the default target variance. The reason for this is to prevent expending computational resources on the initial model and in turn, better employ them when promising regions of exploitation are identified.

After the construction of the SK metamodel for the initial sampling plan, the infill stage begins. The AEI method, presented in subsection 3.3, is employed for this purpose. Here, an initial target variance  $\bar{\sigma}_{target}^2$  is

set and the first infill point is added to the model being simulated up to this corresponding target variance.

From the second infill point on, the adaptive target selection scheme starts to take place. We propose the use of an exponential decay equation parametrized by problem dimension ( $n$ ) and the number of points already sampled near the new infill point ( $n_{close}$ ). The latter is defined by the number of points in the model located at a given distance of the infill point. Suppose  $\mathbf{q}$  is the point that maximizes the infill criterion. We propose to evaluate  $n_{close}$  as

$$n_{close} = \sum_{j=1}^{n_s} I(\mathbf{q}, \mathbf{d}^{(j)}), \quad (16)$$

where

$$I(\mathbf{q}, \mathbf{d}^{(j)}) = \begin{cases} 1, & \|\mathbf{q} - \mathbf{d}^{(j)}\| \leq r_{hc}, \\ 0, & \|\mathbf{q} - \mathbf{d}^{(j)}\| > r_{hc}, \end{cases} \quad (17)$$

in which  $\|\cdot\|$  is a given vector norm and  $r_{hc}$  is one of the input parameters of the proposed approach and corresponds to the distance considered around the infill point.

For evaluation of Eq. (16) we take, without loss of generality, the maximum vector norm. For an arbitrary vector  $\mathbf{u}$ , it is given by

$$\|\mathbf{u}\| = \max_{i=1,2,\dots,n} |u_i|, \quad (18)$$

and thus we consider a hypercube around the infill point selected with half-sides  $r_{hc}$ . Intuitively, this parameter controls the aggressiveness of the search. Increasing it makes the hypercube larger, allowing more sampled points to be treated as close ones.

Then, when the infill is located within an unsampled region, its target variance is set as the initial target variance. On the other hand, when the infill is located in a region with existing sampled points, a lower target variance ( $\bar{\sigma}_{adapt}^2$ ) is employed for the approximation of its objective function value. This is done to allocate more computational effort on regions that need to be exploited. Thus, it indicates the purpose of the infill. Isolated infill points focus on exploring the landscape, where higher MCI accuracy is not needed. When they start to group up, the focus changes to landscape exploitation. In this situation, the target MCI variance is set to a lower value, increasing the model accuracy. By doing so, it also avoids the clustering of multiple inaccurate points that causes the stalling observed in Fig. 5.



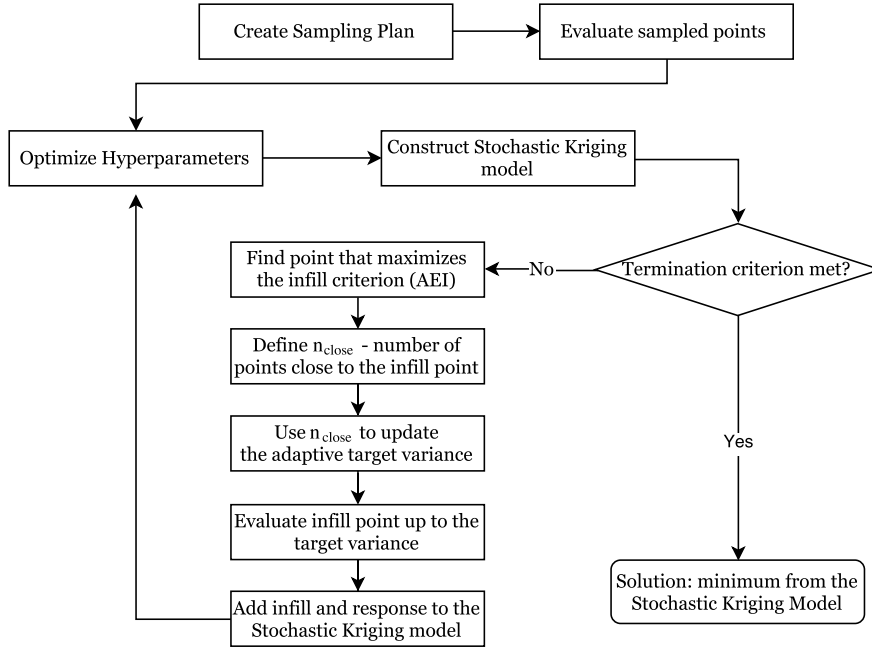


Fig. 6 Flowchart of the algorithm

Since different targets are being employed,  $\lambda$  becomes dependent on the sampling characteristics. It is now adaptively updated according to

$$\lambda(\mathbf{d}) = \begin{cases} \bar{\sigma}_{target}^2 & \text{if } \mathbf{d} \in \mathbf{I} \text{ and } n_{close} = 0 \\ \bar{\sigma}_{adapt}^2 & \text{if } \mathbf{d} \in \mathbf{I} \text{ and } n_{close} > 0, \\ \bar{\sigma}_{target}^2 & \text{if } \mathbf{d} \notin \mathbf{I} \end{cases} \quad (19)$$

where  $\bar{\sigma}_{target}^2$  is the initial target variance and  $\bar{\sigma}_{adapt}^2$  is the adaptive target variance. The value of  $\bar{\sigma}_{adapt}^2$  is then set in order to ensure that points in regions already sampled have a low target variance, in order to exploit a promising region accurately.

In this paper, the expression proposed to calculate the adaptive target value for each iteration of the sEGO algorithm is

$$\bar{\sigma}_{adapt}^2 = \bar{\sigma}_{target}^2 \exp(-g(n, n_{close})), \quad (20)$$

where  $g$  is a function that depends on the problem dimension ( $n$ ) and  $n_{close}$ . The reasoning behind the construction of Eq. (20) is twofold:

- *it displays an exponential decay of the target value:* the choice of an exponential decay seems to be the most intuitive considering how the number of function evaluations increases and the error decreases. If a linear model were used instead, the target would decrease very slightly with few closer points. Yet,

it would drop abruptly as  $n_{close}$  increased, reaching the lower bound for the target. This would cause, initially, an unnecessary number of infill points added to the model without a reasonable gain of information. Further in the optimization, the target would drop abruptly resulting in a large number of evaluations. With the proposed approach, the target starts with high values and is progressively lowered when points begin to cluster around an optimum valley.

- *the decay rate is proportional to the problem dimension  $n$ :* with low dimensional problems, the design space is relatively small so that it becomes easier for the infill points to cluster. Thus, the targeting decay cannot be too aggressive at risk of expending too much computational resources. At higher dimensions,  $n_{close}$  does not increase so fast. Thus, it allows for a more significant target decay. Hence, it indicates the necessity of  $g$  to depend on  $n$ .

In all the examples of this paper, we employ:

$$g(n, n_{close}) = a_1 + a_2 \cdot n + a_3 \cdot n_{close} - a_4 \cdot n_{close} \cdot n, \quad (21)$$

where  $a_i$  are given constants. Figure 7 presents the logarithmic scale plot of Eq. (20) for different problem dimensions using  $a_1 = a_2 = a_3 = 1/2$  and  $a_4 = 1/100$ .

It is worth to highlight here that it is also important to set a minimum value for the adaptive target to avoid a computationally intractable number of samples.

In other words, not to spend the entire computational budget in only a few points. We thus enforce

$$\bar{\sigma}_{\min}^2 \leq \bar{\sigma}_{\text{adapt}}^2 \leq \bar{\sigma}_{\text{target}}^2, \quad (22)$$

where  $\bar{\sigma}_{\min}^2$  is a lower bound on the target.

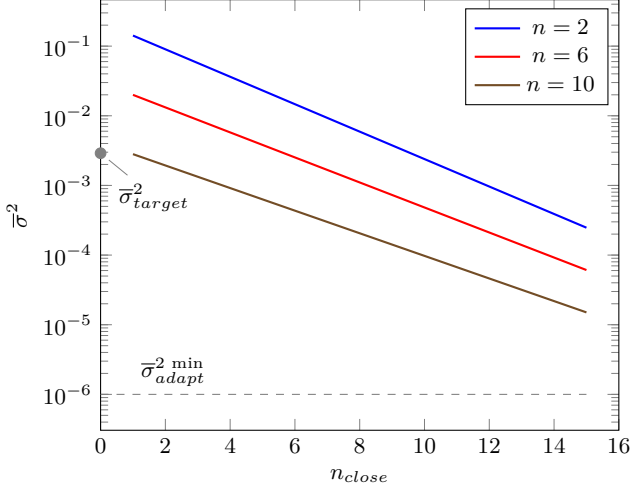


Fig. 7 Target decay varying with problem dimension

## 6 Numerical Examples

In this section, the performance of the proposed approach is evaluated by the solution of stochastic versions of global optimization benchmark test functions. These functions possess a single global optimum and most of them are multimodal, making them good candidates to assess the method’s exploration and exploitation capabilities. These stochastic versions are constructed by inserting multiplicative random variables into the functions. The random variables follow known distributions with specified parameters for each problem.

Here, the efficiency of each algorithm is measured by the number of function evaluations (NFE), *i.e.* the number of times the function  $\phi$  is evaluated, which also is employed as the stopping criterion in all the examples. Hence, once the maximum NFE is reached, the algorithm is stopped and the current best design is set as the optimum design of the search. Since the benchmark functions are not expensive to evaluate, it becomes pointless to discuss computational effort as measured in processing time. For this reason, this information is not presented.

It is important to point out that the optimization procedure presented depends on random quantities. Therefore, the results obtained are not deterministic and may

change when the algorithm is run several times. For this reason, when dealing with stochastic algorithms, it is appropriate to present statistical results over a number of algorithm runs (Gomes et al., 2018). Thus, for each problem, the average as well as the 5 and 95 percentiles of the results found over the set of 100 independent runs are presented. These percentiles are represented by the error bars in the figures. These error bars may be seen as a robustness measure of each algorithm, *i.e.* its ability to provide reasonable results independently of the seed of the random number generator.

Regarding Kriging, for the MLE optimization step, PSO with the default parameters from the Matlab (Mat, 2015) implementation was employed. For the AEI infill criterion,  $\alpha = 1.00$  was used as suggested by Huang et al. (2006).

In subsection 6.1, we compare the constant and the proposed adaptive variance target selection while subsection 6.2 aims to compare the proposed scheme against a multi-start algorithm.

### 6.1 Stochastic EGO: adaptive against constant target

In this section, we present the numerical examples in increasing order of complexity, *i.e.* we investigate problems with 1 to 10 design variables. For the proposed adaptive target selection, we employ the framework described in Fig. 6, while for the constant target value,  $\bar{\sigma}_{\text{target}}^2$  is set constant throughout the search. In the examples presented in the next subsections, we also evaluate the efficiency of these methods for different input random variables levels by varying their standard deviation. It is important to remark that a different initial sampling plan is employed for each independent run of the algorithm. However, the same initial sampling plans are used for both constant and adaptive targeting to keep a fair comparison between them.

For the upcoming examples, the following parameters are kept constant: initial sampling plans comprised of  $n_s = 7n$  points,  $r_{hc} = 0.1$ ,  $a_1 = a_2 = a_3 = 1/2$  and  $a_4 = 1/100$ ,  $\bar{\sigma}_{\min}^2 = 10^{-6}$ , and for the adaptive scheme, the initial variance target value is set as  $\bar{\sigma}_{\text{target}}^2 = 1.0$ .

It is worth to highlight that all the parameters of the proposed adaptive approach are kept constant throughout this section. By doing this, we aim to evaluate whether the proposed adaptive approach is able to reach reasonable results without having to tune its parameters.

#### 6.1.1 Multimodal 1D problem

Consider the multimodal 1D problem, given by Eqs. (14) and (15), presented in Section 4. We employ the

MCI to approximate the integral in Eq. (15) and the proposed sEGO scheme to search for  $d^*$ . Here, we solve this problem for two different standard deviation levels, *i.e.*  $\sigma_X = 0.2$  and  $0.3$ , and three different values of the stopping criterion, *i.e.*  $\text{NFE} = 50, 100, 150$ .

In this example, we first highlight the difficulty of setting a constant target variance. Hence, Fig. 8 presents the results of the constant approach using different values of  $\bar{\sigma}_{\text{target}}^2 = 1.0, 10^{-1}, 10^{-2}, 10^{-3}, 10^{-4}$ , and using  $\text{NFE} = 150$  as stopping criterion. It is easily noticeable from these results that the performance and robustness of the algorithm is highly dependent on the value of  $\bar{\sigma}_{\text{target}}^2$ . For example, for the case  $\sigma_X = 0.2$ , the best constant variance is  $\bar{\sigma}_{\text{target}}^2 = 10^{-2}$  as shown in Fig. 8a, while for  $\sigma_X = 0.3$ , both  $\bar{\sigma}_{\text{target}}^2 = 10^{-1}$  and  $\bar{\sigma}_{\text{target}}^2 = 10^{-2}$  could be considered good constant targets, as shown in Fig. 8b. It puts in evidence the necessity of an adaptive target variance selection scheme.

Figure 9 presents the results comparing the constant and adaptive target approaches for different standard deviation values of the input random variable: (a)  $\sigma_X = 0.2$  and (b)  $\sigma_X = 0.3$ . Here, we employ for the constant target scheme,  $\bar{\sigma}_{\text{target}}^2 = 10^{-3}$ . In this figure, the height of the bars represent the average solution found over 100 independent runs of the algorithm, while the error bars illustrate the dispersion of the results (5 and 95 percentiles).

For the case in which  $\sigma_X = 0.2$ , the adaptive approach presented a good performance from the lowest NFE considered, while the constant approach performed better as the computational budget was increased. In the case with higher noise ( $\sigma_X = 0.3$ ), the adaptive approach provided a better value of the mean value of the independent runs as well as lower dispersion. The results presented in this example show that the proposed adaptive target approach successfully minimized Eq. (15), and presented clear advantage over the constant approach, especially in the case of higher variability of the input random parameter.

### 6.1.2 Multimodal 2D problem

In the same manner as the previous subsection, we consider a multimodal stochastic two dimensional function:

$$\phi(\mathbf{d}, \mathbf{X}) = p_1(d_2 - p_2d_1^2 + p_3d_1 - p_4)^2X_1 + p_5(1 - p_6)\cos(d_1)X_2 + p_5 + 5d_1, \quad (23)$$

with parameters  $p_1 = 1$ ,  $p_2 = 5.1/(4\pi^2)$ ,  $p_3 = 5/\pi$ ,  $p_4 = 6$ ,  $p_5 = 10$ ,  $p_6 = 1/(8\pi)$ . The design domain is  $S = \{d_1 \in [-5, 10], d_2 \in [0, 15]\}$ .

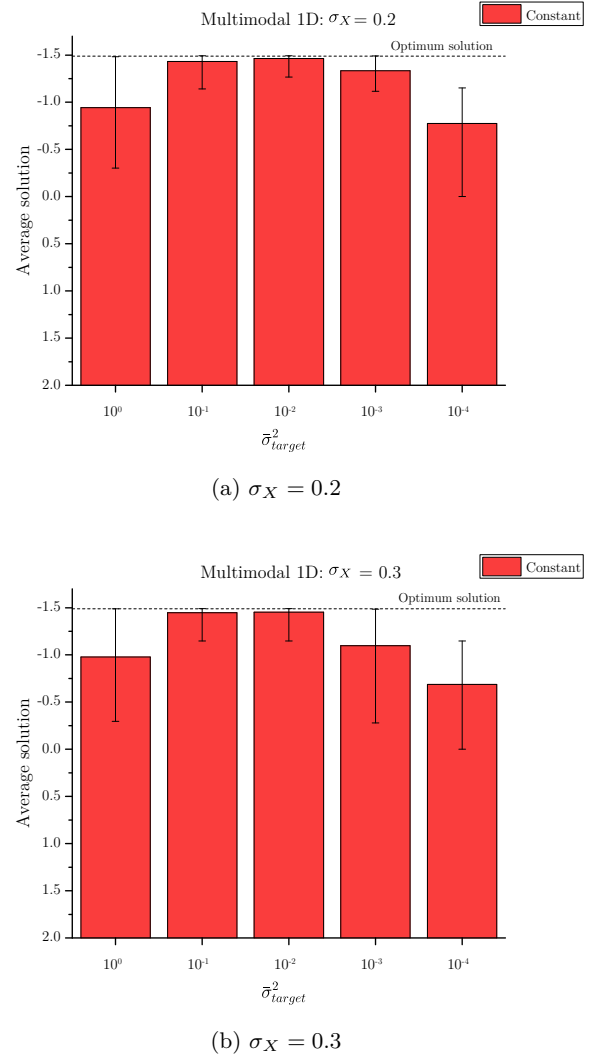


**Fig. 8** Multimodal 1D problem: results of constant approach for different values of  $\bar{\sigma}_{\text{target}}^2$

$X_1$  and  $X_2$  are Normal random variables given by  $(X_1, X_2) \sim \mathcal{N}(1, \sigma_X)$ . The weight function  $w$  from Eq. (1) is taken as the probability density function (PDF)  $f_{\mathbf{X}}(\mathbf{x})$  of the random vector  $\mathbf{X} = \{X_1, X_2\}$ . The integral from Eq. (1) then becomes the expected value of  $\phi$  and we have the optimization problem

$$\min_{d \in S} J(\mathbf{d}) = \mathbb{E}[\phi(\mathbf{d}, \mathbf{X})] = \int_{\Omega} \phi(\mathbf{d}, \mathbf{x}) f_{\mathbf{X}}(\mathbf{x}) d\mathbf{x}, \quad (24)$$

where  $\Omega = \mathbb{R}^{n_x}$  is the support of  $f_{\mathbf{X}}(\mathbf{x})$ .

In this problem,  $\phi(\mathbf{d}, \mathbf{X})$  is a modified Branin function where a term  $5d_1$  is added to the function. This modification forces the existence of a single global optimum value. The plot of the deterministic version of this function is shown in Fig. 10.

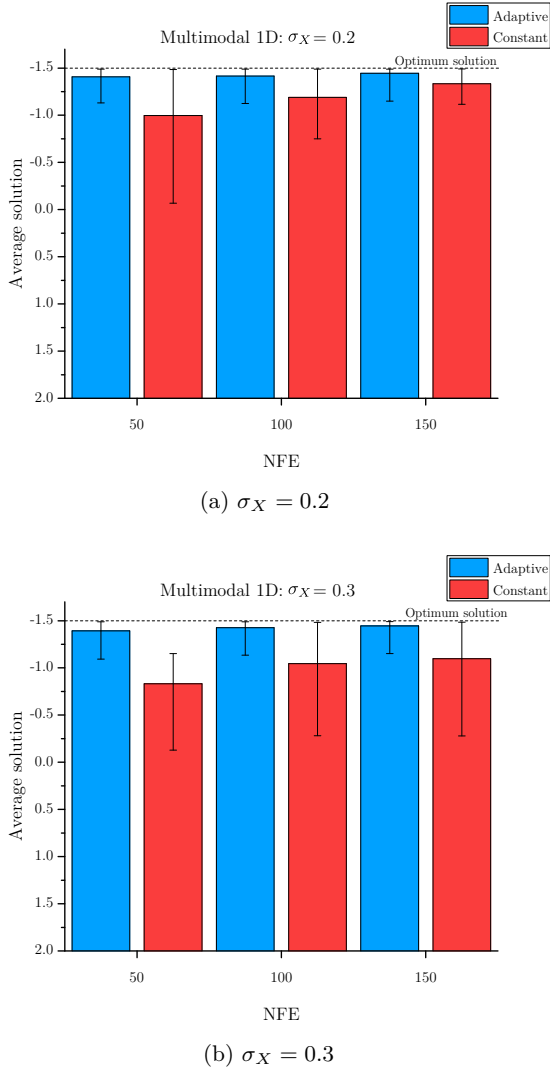


**Fig. 9** Multimodal 1D problem: results of the adaptive and constant target selection approaches

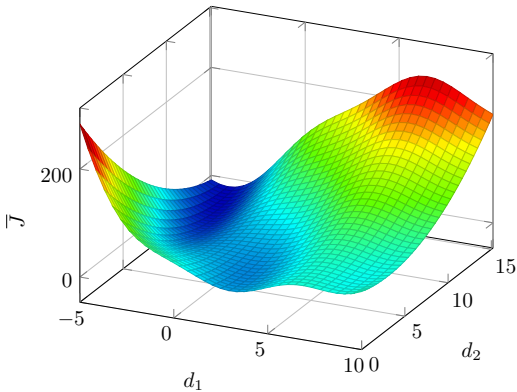


**Fig. 10** Function plot - Branin tilted

Two cases are considered for different standard deviation values of the input random variable: (a)  $\sigma_{\mathbf{X}} = 0.01$  and (b)  $\sigma_{\mathbf{X}} = 0.05$ , and three different values of the stopping criterion, *i.e.* NFE = 100, 300, 1000. It should be remarked that the behavior of the constant approach is quite similar to the one presented in the previous example, *i.e.* the robustness and performance are highly dependent on the value of  $\bar{\sigma}_{target}^2$ . Hence, we only present from here on the most reasonable results reached by this method. In this example, they are given by  $\bar{\sigma}_{target}^2 = 10^{-2}$ .

Figure 11 presents the results comparing the constant and adaptive target approaches. It can be observed that the proposed adaptive approach once more provided better average values and lower dispersion over the independent runs when compared to the constant target approach. Furthermore, in this problem, the adaptive approach provided better results even for the lower noise situation ( $\sigma_{\mathbf{X}} = 0.01$ ). The only exception was for  $\sigma_{\mathbf{X}} = 0.05$  with NFE=100, where the constant approach presented better results than the adaptive one, as shown in Fig. 11(b).

### 6.1.3 Multimodal 6D problem and high stochastic dimension

This multimodal benchmark function has six local minima and one global minimum. It is the well-known Hartman 6D deterministic benchmark function modified by stochastic multiplicative coefficients in the following form:

$$\phi(\mathbf{d}, \mathbf{X}) = - \sum_{i=1}^4 p_i \exp \left( - \sum_{j=1}^6 A_{ij} (d_j X_j - P_{ij})^2 \right), \quad (25)$$

where

$$\mathbf{p} = [1.0, 1.2, 3.0, 3.2]^T, \quad (26)$$

$$A = \begin{bmatrix} 10 & 3 & 17 & 3.50 & 1.7 & 8 \\ 0.05 & 10 & 17 & 0.1 & 8 & 14 \\ 3 & 3.5 & 1.7 & 10 & 17 & 8 \\ 17 & 8 & 0.05 & 10 & 0.1 & 14 \end{bmatrix} \quad (27)$$

and

$$\mathbf{P} = 10^{-4} \begin{bmatrix} 1312 & 1696 & 5569 & 124 & 8283 & 5886 \\ 2329 & 4135 & 8307 & 3736 & 1004 & 9991 \\ 2348 & 1451 & 3522 & 2883 & 3047 & 6650 \\ 4047 & 8828 & 8732 & 5743 & 1091 & 381 \end{bmatrix}. \quad (28)$$

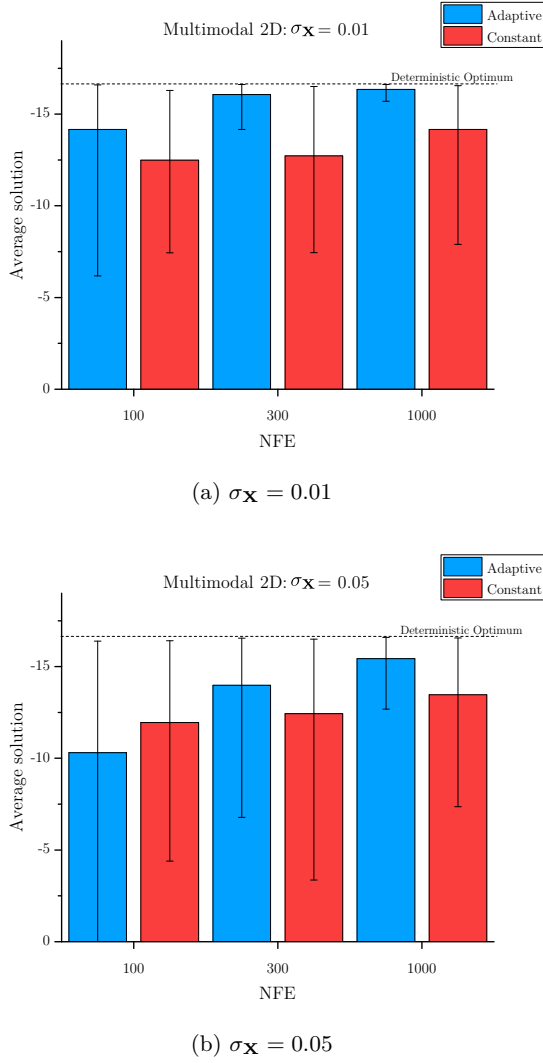


**Fig. 11** Multimodal 2D problem: results of the adaptive and constant target selection approaches

The design domain is defined as the unit hypercube  $S = \{d_i \in [0, 1], i = 1, 2, \dots, 6\}$ . In the following, we analyzed two cases of the Hartman function with different stochastic dimensions: Case 1 with  $n_x = 6$ , and Case 2 with  $n_x = 54$ .

#### Case 1: $n_x = 6$

The random variables  $X_i$  have Normal distribution  $X_i \sim \mathcal{N}(1, \sigma_X)$ . The weight function from Eq. (1) is again taken as the PDF of the random variables and thus the objective function becomes the expected value of  $\phi$ . The resulting optimization is then as presented in Eq. (24).

For this problem constant and adaptive approaches are compared for the following standard deviation values of the input random variable: (a)  $\sigma_{\mathbf{X}} = 0.05$  and (b)  $\sigma_{\mathbf{X}} = 0.1$ . Moreover, three different values of the

stopping criterion were considered:  $\text{NFE} = 50, 100, 150$ . Finally,  $\bar{\sigma}_{\text{target}}^2 = 10^{-3}$  is employed for the constant target approach.

Figure 12 presents the results for both cases analyzed. In all the cases, the proposed adaptive approach obtained better results. As the dispersion of the input random variables increases, it takes more samples to reach a certain variance target, becoming prohibitive to expend the computational budget on accurate exploration points. Consequently, the adaptive target setting enables the optimization to run longer than the constant approach. That is, since the adaptive approach *spends* the available computational budget more rationally, it enables the search to visit more regions on the domain, providing better results.

Without the early termination proposed in the benchmark, a small constant target would try to reduce the model uncertainty over the whole design domain instead of only on the promising regions.

#### Case 2: high stochastic dimension $n_x = 54$

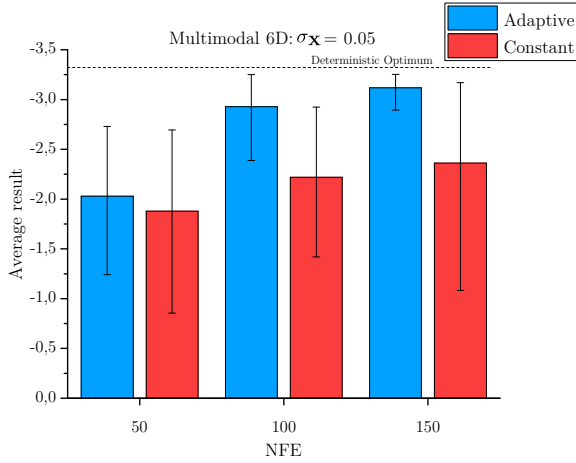
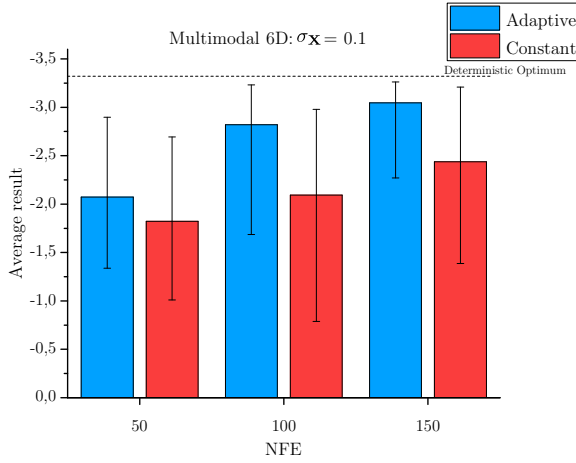
This case aims at investigating the performance of the proposed approach in problems with high stochastic dimension ( $n_x$ ). For this purpose, the six random variables of case 1 are kept and we also model all the elements of matrices  $\mathbf{A}$  and  $\mathbf{P}$  as independent normal random variables. More specifically,  $(\mathbf{A})_{ij} = A_{ij} \cdot \mathcal{N}(1, \sigma_A)$  and  $(\mathbf{P})_{ij} = P_{ij} \cdot \mathcal{N}(1, \sigma_P)$ , where  $\sigma_A$  and  $\sigma_P$  are both 0.01.

Figure 13 presents the results from the analysis of Case 2. Worse results than those obtained from Case 1 are expected as we are dealing with a higher number of stochastic variables. Moreover, the same number of evaluations was employed for the stopping criterion, in order to enable direct comparison. Nevertheless, the adaptive procedure presented better results than the constant case. Additionally, variability of the adaptive results decreased with the increase of NFE, showing a convergence pattern. This case illustrates the promising use of the proposed adaptive approach for problems with a high number of stochastic dimensions.

#### 6.1.4 Multimodal 10D problem

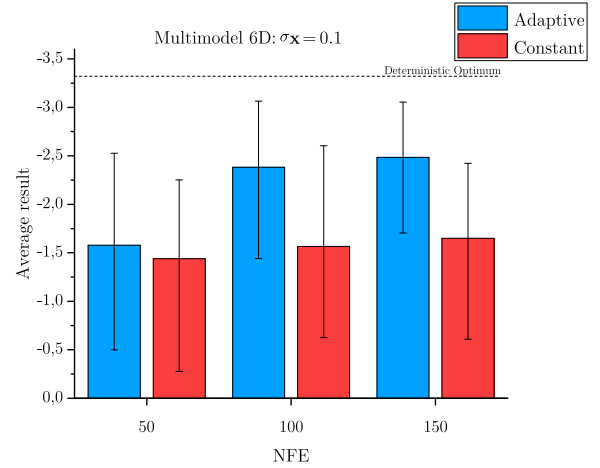
The last benchmark problem is a stochastic version of the Levy function, which is the following  $n$ -dimensional multimodal benchmark problem:

$$\begin{aligned} \phi(\mathbf{d}, \mathbf{X}) = & \sin^2(\pi p_1) + \sum_{i=1}^{n-1} (p_i - 1)^2 [1 + 10 \sin^2(\pi p_i + 1)] \\ & + (p_n - 1)^2 [1 + \sin^2(2\pi p_n)], \end{aligned} \quad (29)$$

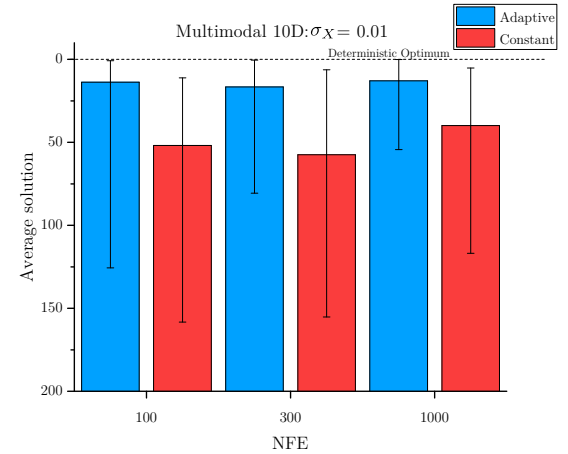
(a)  $\sigma_X = 0.05$ (b)  $\sigma_X = 0.1$ **Fig. 12** Multimodal 6D problem: results of the adaptive and constant target selection approaches

where  $p_i = 1 + \frac{d_i X_i}{4}$  for  $i = 1, 2, \dots, n$ . Here we take  $n = 10$  and a design domain  $S = \{d_i \in [-10, 10], i = 1, 2, \dots, 10\}$ . The random variables  $X_i$  follow a Normal distribution with  $\sigma_X = 0.01$ , *i.e.*,  $X_i \sim \mathcal{N}(1, 0.01)$ . As we did in the previous examples, the weight function is taken as the PDF of the random vector and the problem is written as the minimization of the expected value of  $\phi$ , as presented in Eq. (24). Here, three different values of the stopping criterion were considered: NFE = 50, 100, 150, and we set  $\bar{\sigma}_{target}^2 = 10^{-2}$  for the constant target approach.

The results are presented in Fig. 14. Similarly to the previous example, the adaptive targeting obtains better average results than the constant counterpart. Moreover, increasing the maximum number of function evaluations consistently decreases the variability of results, represented by the error bars. The method ob-

**Fig. 13** Multimodal 6D problem: higher number of stochastic dimensions

tain reasonable results using a relatively small number of function evaluations even considering a very large 10-dimensional design space.

**Fig. 14** Multimodal 10D problem: results of the adaptive and constant target selection approaches

## 6.2 Adaptive approach against multiple start optimization methods

It became clear from the previous examples that the proposed adaptive sEGO algorithm can be successfully employed in the optimization of problems of the sort of Eq. (1). However, when investigating the performance of global optimization algorithms, it is desirable to present a comparison with multi-start based approaches (Le Riche and Haftka, 2012). Hence, in this section, we make a comparison with the Globalized

Bounded Nelder–Mead (GBNM) algorithm (Luersen and Le Riche, 2004), which consists of a probabilistic restart procedure coupled with a Nelder–Mead local search (Nelder and Mead, 1965). The GBNM was successfully applied to several multimodal problems in engineering, such as laminated composite structures (Luersen et al., 2004), truss optimization (Torii et al., 2011), rotor robust design (Ritto et al., 2011; Lopez et al., 2014), damage identification (Miguel et al., 2013; Nhamage et al., 2016), among others. Further details on the algorithm are presented in Appendix C.

### 6.2.1 Adaptive target and GBNM with fixed size sample

In order to set the sample size in Eq. (2) for the GBNM, we employ the following procedure widely adopted in the literature of robust design (Capiez-Lernout and Soize, 2008; Soize et al., 2008; Ritto et al., 2011; Lopez et al., 2014; Fadel et al., 2016; Miguel et al., 2016). First, we construct a convergence plot of  $\bar{J}$  with respect to the sample size employed in MCI. Then, we set  $n_r$  as the sample number around the value that  $\bar{J}$  becomes stable. For example, Fig. 15 shows an example of the convergence curve of  $\bar{J}$  in a given point of the design domain of the multimodal 1D problem.  $\bar{J}$  becomes stable after approximately 100 simulations is employed in MCI. Hence, we set  $n_r = 100$ , keeping it constant throughout the search, and sample  $\mathbf{x}^{(i)}$  always using the same seed of the random number generator.

Regarding computational cost, however, note that this is the same multimodal 1D function that we optimized in section 6.1.1, whose results are in Fig. 9. If 100 simulations were employed for each new point required by the GBNM algorithm, the computational cost would be much higher than the  $\text{NFE} = 150$  stopping criterion employed with the proposed approach. Consequently, the proposed approach is much more efficient than any algorithm similar to the GBNM in this problem if this fixed size sample method is employed to obtain  $\bar{J}$ . Furthermore, the same conclusion may be drawn if we apply this procedure to the other benchmark problems analyzed in Section 5.1. Hence, this analysis is not presented for them here.

### 6.2.2 sEGO and GBNM with constant target variance

Consider again the 1D problem from section 6.1.1. We now set the same target variance for both algorithms, GBNM and constant approach. That is, we set  $n_r$  as the sample size that provides  $\bar{\sigma}_{\text{target}}^2 = 10^{-3}$ , and the stopping criterion as the maximum number of NFE like the previous section. Two cases are analyzed: (a)

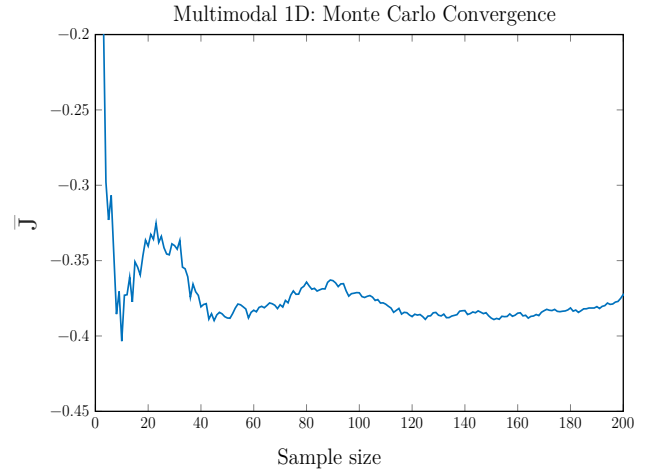


**Fig. 15** Mean convergence for Multimodal 1D function

$\sigma_X = 0.2$  and (b)  $\sigma_X = 0.3$ , and Fig. 16 presents the obtained results for the sEGO approaches and GBNM.

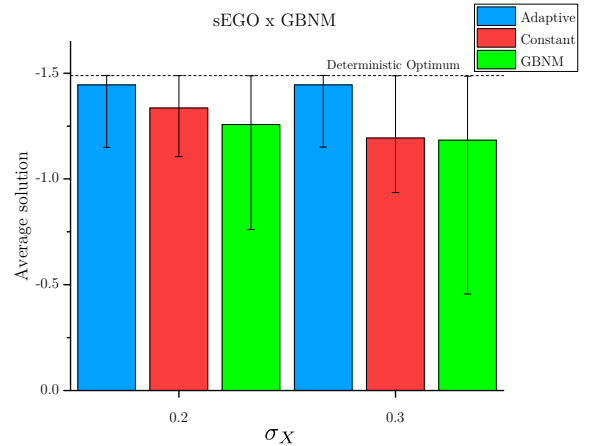


**Fig. 16** Comparison between sEGO and GBNM for the Multimodal 1D function

In case (a) ( $\sigma_X = 0.2$ ), it can be seen that the sEGO algorithm display a lower dispersion of the results as well as lower objective function value. For the  $\sigma_X = 0.3$  case, the maximum number of evaluations differs in each method. For sEGO, we maintain  $\text{NFE} = 150$ , while for GBNM, we increase NFE to 1000. This is done because if we set  $\text{NFE} = 150$ , GBNM does not provide reasonable results. By comparing both approaches in this case (Fig. 16), it can be seen that GBNM provides even more spread results, while sEGO obtain results closer to the optimum solution, especially for the proposed adaptive approach.

This behavior persists and is largely amplified when the problem dimension increases. This leads to an even



higher discrepancy between the sEGO approaches (constant and adaptive target) and GBNM. Thus, further examples in higher dimensions are not shown. The results of this section indicate that the sEGO approaches largely outperform multi-start based methods for problems of the sort of Eq. (1).

### 6.3 Application: Tuned-Mass Dumper (TMD) system optimization

As discussed in section 2, there are several engineering problems where the proposed integral minimization could be employed. In this section, one application in the field of structural dynamics is shown. It involves the seismic vibration control of a structure. The optimization problem resumes to determine the stiffness and damping of a TMD device in order to maximize the structural reliability of a building subject to seismic excitation (Chakraborty and Roy, 2011). The problem is briefly presented in the next paragraphs. For a more detailed description, the reader is referred to Lopez et al. (2015). It should be noted that the problem presented here is strictly academic. Aspects of the real structure are not taken into account and simplifications were made such as: assuming the structural response linear elastic, the excitation comes from a stationary process, the random variables of each floor are uncorrelated, *etc.* Nevertheless, it remains as a fairly complex problem comprehending the engineering fields of optimization, control, dynamics and reliability.

Consider the  $N$ -story Multiple Degrees of Freedom (MDOF) linear building structure with a TMD installed at the top floor illustrated in Fig. 17. The equation of motion of the combined system subject to ground acceleration can be written as

$$\mathcal{M}\ddot{\mathbf{z}}(t) + \mathcal{C}\dot{\mathbf{z}}(t) + \mathcal{K}\mathbf{z}(t) = -\mathbf{m}\ddot{z}_g(t), \quad (30)$$

where  $\mathbf{z}$  is the  $(N+1)$  dimensional response vector representing the displacements relative to the ground

$$\mathbf{z}(t) = \{z_1, z_2, \dots, z_N, z_d\}, \quad (31)$$

$\ddot{z}_g$  is the ground acceleration,  $\mathbf{m}$  is the mass vector

$$\mathbf{m} = \{m_1, m_2, \dots, m_N, m_d\}, \quad (32)$$

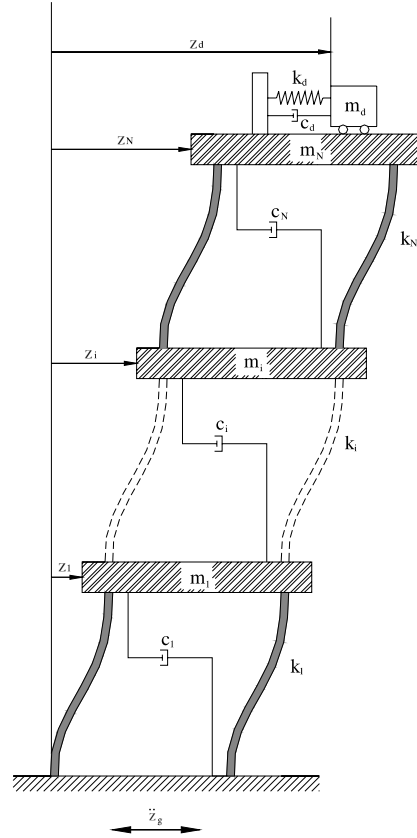


Fig. 17 TMD building

and  $\mathcal{M}$ ,  $\mathcal{C}$  and  $\mathcal{K}$  are matrices corresponding to the mass, viscous damping and the stiffness of the structure, respectively. These matrices can be written as

$$\mathcal{M} = \begin{bmatrix} m_1 & & & \\ & m_2 & & \\ & & \ddots & \\ & & & m_N \\ & & & & m_d \end{bmatrix} \quad (33)$$

$$\mathcal{C} = \begin{bmatrix} (c_1 + c_2) & -c_2 & & & \\ -c_2 & (c_2 + c_3) & -c_3 & & \\ & -c_3 & & & \\ & & \ddots & -c_N & \\ & & -c_N & (c_N + c_d) & -c_d \\ & & & -c_d & c_d \end{bmatrix} \quad (34)$$

$$\mathcal{K} = \begin{bmatrix} (k_1 + k_2) & -k_2 & & & \\ -k_2 & (k_2 + k_3) & -k_3 & & \\ & -k_3 & & & \\ & & \ddots & -k_N & \\ & & -k_N & (k_N + k_d) & -k_d \\ & & & -k_d & k_d \end{bmatrix} \quad (35)$$

where  $m_i$ ,  $c_i$  and  $k_i$  are respectively the mass, damping and stiffness of the  $i$ -th floor, while  $m_d$ ,  $c_d$  and  $k_d$



are respectively the mass, damping and stiffness of the TMD.

We consider in this example that the structure is a ten-story ( $N = 10$ ) shear frame. The height of each floor is 3 meters, resulting in a total height ( $h$ ) of 30 meters. Also, we model  $m_i$ ,  $c_i$  and  $k_i$  ( $i = 1, \dots, N$ ) as Gamma random variables (Ritto et al., 2011) and group them into the random vector  $\mathbf{X}$ . Their mean values and Coefficient of Variation (C.o.V) are in Table 1. Notice here that the stochastic dimension of the problem is  $n_x = 30$ .

**Table 1** Statistical properties of structural parameters

		Mean	C.o.V. [%]
Stiffness [N/m]	Story	$650.0 \times 10^6$	15
	TMD	$k_d$	15
Mass [kg]	Story	$360.0 \times 10^3$	05
	TMD	$108.0 \times 10^3$	05
Damping [Ns/m]	Story	$6.20 \times 10^6$	25
	TMD	$c_d$	25

The earthquake excitation is modeled as a white noise signal with constant spectral density,  $S_0$ , filtered through the Kanai-Tajimi spectrum (Kanai, 1957; Tajimi, 1960). The power spectral density function is given by:

$$s(\omega) = S_0 \left[ \frac{\omega_f^4 + 4\omega_f^2 \xi_f^2 \omega^2}{(\omega^2 - \omega_f^2)^2 + 4\omega_f^2 \xi_f^2 \omega^2} \right], \quad (36)$$

where  $\xi_f$  and  $\omega_f$  are the ground damping and frequency, respectively. Their values are adopted as  $\xi_f = 0.6$ ,  $\omega_f = 37.3 \text{ rad/s}$  (Mohebbi et al., 2013). The term  $S_0$  acts as a scaling factor and in this context represents the amplitude of the bedrock excitation spectrum. Its value is adopted as  $S_0 = 1 \times 10^{-3} \text{ m}^2/\text{s}^3$ . This combination of parameters corresponds to an earthquake with 0.38g peak ground acceleration on a medium firm soil (Chen and Lui, 2005). The solution of the equation of motion is based on the Lyapunov equation. By solving the Lyapunov equation of the problem for the covariance matrix, it is possible to extract the variance of the displacements and velocities from each degree of freedom. Therefore, it becomes straightforward to calculate the standard deviation of those quantities, which are in turn needed for the reliability index computation. For a description of this procedure, the reader is referred to Mantovani et al. (2017).

The evaluation of the structural reliability ( $\bar{\beta}$ ) leads to a time dependent reliability problem. Here, we employ the out-crossing rate approach for this purpose,

which is detailed in Appendix B. For the calculation of the reliability index  $\bar{\beta}$ , the design life time ( $t_D$ ) of the structure is considered to be 50 years. Moreover, the rate of arrival ( $\nu$ ) of earthquake events is of 1 every 10 years and each event had the duration  $t_E$  of 50 seconds. In this example, the top floor maximum displacement is chosen as failure criterion. Three different cases of failure barrier levels are analyzed: (a)  $b = h/300$ , (b)  $b = h/400$ , (c)  $b = h/500$ .

Thus, considering the design vector  $\mathbf{d} = [k_d, c_d]$  and the stochastic parameters vector  $\mathbf{X}$ , the problem can be stated:

$$\min_{\mathbf{d} \in S} J(\mathbf{d}) = -\bar{\beta}(\mathbf{d}), \quad (37)$$

in which the minus sign leads to the maximization of  $\bar{\beta}$ , which is given by Eq. (54). The design domain  $S$ , comprises the lower and upper bounds on the stiffness ( $k_d$ ) and damping coefficient ( $c_d$ ) of the TMD. The bounds have values of  $[0, 4000]$  kN/m and  $[0, 1000]$  kNs/m, respectively.

In Fig. 18 it can be seen how irregular the surface becomes when considering the output without simulation, *i.e.* the result of a single evaluation for each input.

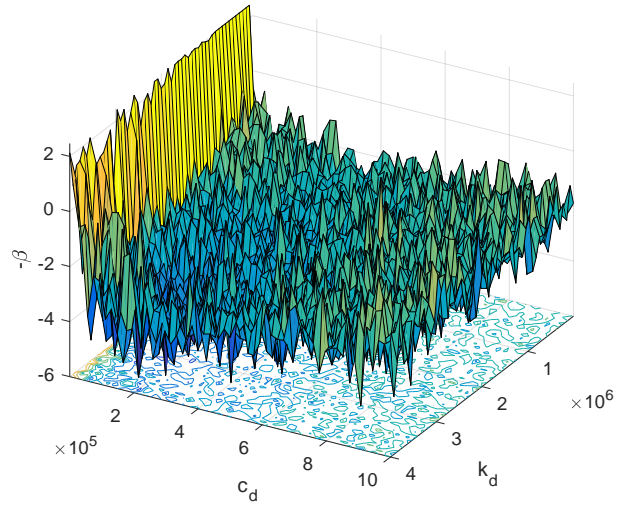


**Fig. 18** Noisy reliability surface over design variables range

Table 2 presents the optimization results using the proposed sEGO approach with adaptive target variance. The stopping criterion of the algorithm is the maximum number of calls of the FE code, *i.e.* NFE=1000. The stiffness ( $k_d$ ) and damping ( $c_d$ ) are displayed along with the best ( $\bar{\beta}_{\max}$ ) and average ( $\bar{\beta}_{\text{ave}}$ ) results found over 25 independent runs of the algorithm. For comparison, the reliability index for the uncontrolled case is also displayed.

It can be seen that smaller barrier level results in smaller values of  $\bar{\beta}$ , thus increasing the failure probability. Notable increases in  $\bar{\beta}$  were achieved. Taking for example the case (b), the system reliability increases from 1.37 without TMD to 4.24 by using the TMD with the reported parameters. In terms of failure probability, it means decreasing  $P_f$  from  $8.5 \times 10^{-2}$  to  $1.1 \times 10^{-5}$ . Looking at case (c), the structure that would certainly fail without TMD achieves a reliability index of 2.48 ( $6.6 \times 10^{-3}$  failure probability) when using the optimized TMD parameters. Moreover,  $\bar{\beta}_{\max}$  results remained close to  $\bar{\beta}_{\text{ave}}$ . It indicates the robustness of the proposed approach, *i.e.* it is able to obtain reasonable results in multiple runs despite the large number of random parameters and limited number of function evaluations.

In Fig. 19, the Monte Carlo convergence for a single input is shown. The average value of  $-\bar{\beta}$  starts to converge around 150 simulations. Thus, it becomes clear that applying the standard approach of using this fixed number to simulate every input would lead to a higher computational cost. Simulating only seven different points would cause the maximum number of evaluations of 1000 to be exceeded. However, using the proposed approach only points closer to the optimum are simulated with higher  $n_s$ . Moreover, by employing the regression framework of SK using Monte Carlo variance estimates, one can approximate the underlying global behavior of the problem, avoiding further computational costs.

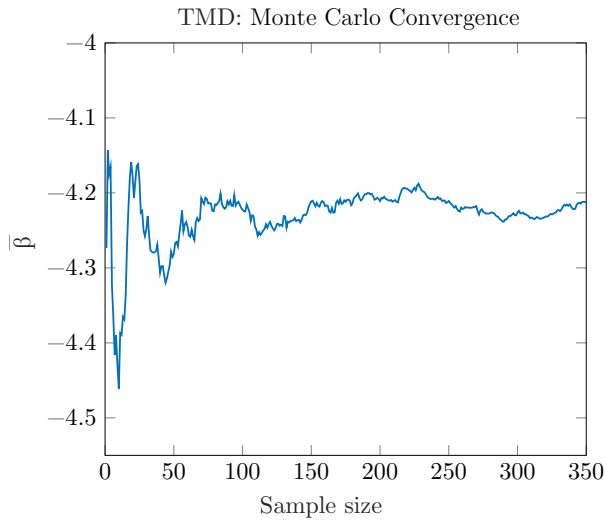


**Fig. 19** Mean convergence for the TMD reliability function

In Fig. 20, the resulting surface generated by the proposed algorithm, considering the case (b) barrier level is illustrated. Comparing it against Fig. 18 shows

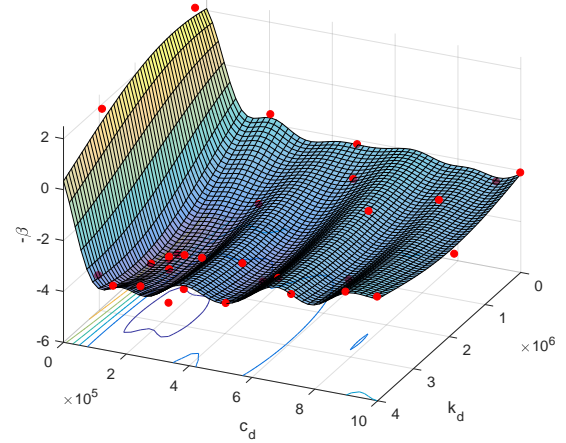


**Fig. 20** Surface generated by Stochastic Kriging with sampled points

how the surface becomes smooth by the regression capabilities of SK. The red dots in Fig. 20 represent the points that were sampled. Some are scattered over the domain, which show the exploration part of the algorithm. Yet, numerous points are concentrated close to minimum value of  $-\bar{\beta}$ , which exploited the region where the global optimum is located. Those are the points obtained by the infill step, with the maximization of the AEI criterion and considering adaptive variance target. This application possess the characteristics which the proposed algorithm is particularly efficient at solving, *i.e.*, problems with numerous random variables but a relatively small number of design variables ( $n \leq 10$ ).

#### 6.4 Further comments

The purpose of this section is offering general guidelines on parameter settings and discussing further application contexts. Overall most parameters remained constant throughout the analysis, where the biggest impact on the performance of the approach certainly comes from enforcing bounds on the target variance with  $\bar{\sigma}_{\text{target}}^2$  and  $\bar{\sigma}_{\text{min}}^2$ . The practical consideration is having an inexpensive upper bound and a limiting lower bound that assures that number of evaluations for each infill point can be completed and is compatible with the given computational budget. The actual values depend on characteristics of the problem being analyzed, where prior testing may be necessary to select reasonable parameters. The parameters of the exponential curve in Eq. (20) remained constant across multiple dimensional problems and should not need major modifications. A side-length  $r_{hc}$  of 10 % of the range of each dimension seemed reasonable given that variables are normalized,

**Table 2** TMD optimization results

Barrier	$k_d(MN/m)$	$c_d(MNs/m)$	$\beta_{max}$	$\beta_{mean}$	$\beta_{uncontrolled}$
(a) h/300	3.053	0.153	6.68	6.31	3.70
(b) h/400	2.963	0.152	4.24	3.99	1.37
(c) h/500	3.018	0.160	2.48	2.31	fail

performing well when the dimension size increased. The initial sampling plan, employed with  $n_s = 7n$  could be altered depending on the problem dimension and stochastic magnitude. For low error and low dimension, a reduced initial sampling plan would lead to a faster convergence, in reason of the higher probability of finding promising regions early.

Regarding further application, we mentioned in Section 2 that promising areas are robust design, Performance Based Design Optimization and Optimal Experimental Design. In the robust design of mechanical systems, MCI with fixed sample size has been largely employed to approximate the integral of Eq. (1), and metaheuristic algorithms have been widely applied to solve the resulting optimization problem. The coupling between fixed sample MCI and metaheuristic algorithms lead to a huge computational cost. In the case of expensive to evaluate functions, this is exactly what the global optimization approach proposed in this paper aims to avoid: the adaptive scheme avoids the full evaluation of the integral and the sEGO tends to find the global optimal solution requiring a fraction of the computational effort demanded by metaheuristic algorithms. Thus, robust design problems based on minimization of the mean response of the system would perfectly fit the capabilities of the algorithm proposed here.

Only a few papers in the literature addressed Performance Based Design Optimization problems, most likely for its huge computational cost (since it couples time dependent reliability analysis, nonlinear dynamics models and optimization). For example, Beck et al. (2014) simplified the problem to have only two random variables (applying a trapezoid rule for integration) and employed a local optimization algorithm. Spence and Kareem (2014) built an equivalent static problem, but still had to solve a high dimension stochastic integral. The proposed sEGO approach could be employed in both situations: in the first, it would make it possible to consider more structural and loading parameters as random variables as well as to pursue a global optimization search, and in the second, it is likely to reduce the computational burden of the optimization process.

In the case of Optimal Experimental Design problems, we may also find some advantages of the proposed optimization method. The approach proposed by Huan and Marzouk (2013) makes use of polynomial chaos sur-

rogates, which may lose efficiency when the stochastic dimension of the problem increases (unless sparse approaches are employed). Thus, the adaptive approach would be preferred over polynomial chaos surrogates in situations with high stochastic dimension. On the other hand, Beck et al. (2018) employed a Laplace-based importance sampling method to alleviate the computational burden in the evaluation of the Optimal Experimental Design double integral. In this case, it is important to mention that this Laplace-based importance sampling method also provides the variance of the error in the integration. Hence, it can be employed (instead of MCI) together with the sEGO approach proposed here to further reduce the computational cost of the optimization problem. The same could be done with other efficient frameworks such as Multi Level Monte Carlo (Giles, 2008) and Multi index Monte Carlo (Haji-Ali et al., 2016).

## 7 Conclusion

This paper presented an efficient sEGO approach for the minimization of functions that depend on an integral. It was first supposed that this integral could be approximated by MCI, which also provided the variance of the error in the approximation. This information about the error was then included into the SK framework by setting a target variance in the MCI. The AEI infill criterion was employed to guide the addition of new point in the metamodel. It was shown that if we set a large and constant target variance for MCI, it may stall the optimization process. On the other hand, if the target variance was relatively low, the computational cost might become prohibitive. It was then identified that there was room for optimization on the selection of the variance target. Hence, we then proposed an adaptive approach for variance target selection, which is the main contribution of this paper.

In order to assess the effectiveness of the proposed method, numerous benchmark problems were analyzed. The proposed method was first compared to the constant approach on deceptive stochastic benchmark functions from the literature, with up to 10 design variables and up to 54 random variables. The proposed adaptive method obtained better results in almost all analyzed

cases. Moreover, it was observed that higher dimensions and higher noise levels led to a higher difference in the results, favoring the proposed approach when compared to the constant target method.

Then, the sEGO algorithms were compared to a multi-start global optimization method, the GBNM. It was shown that the GBNM provided worse results than the sEGO approaches both in terms of efficiency, with a larger number of evaluations required as well as consistency, with a higher 5 to 95 percentile range over multiple runs.

Finally, the design optimization under uncertainties of a TMD system was analyzed. It consisted of a ten-story shear frame subject to seismic excitation. The problem had thirty random variables and the objective was to maximize the structural reliability by selecting the optimal stiffness and damping of the TMD system. The problem was successfully solved and the best results found were presented. The proposed adaptive approach was able to obtain optimal solutions efficiently and consistently for the three cases analyzed. Moreover, it supported its applicability to problems with high stochastic dimensions.

Overall, the proposed adaptive target sEGO method yielded convincing results for the minimization of integrals. Furthermore, the stochastic dimensions of the integral to be minimized does not impose any limitation since we employed MCI for its approximation. By limitation, we mean that the method does not suffer from exponential increase in complexity when the number of stochastic dimensions is increased, also known as curse of dimensionality. Hence, the proposed sEGO method tends to be robust and efficient for the solution of problems that depend on the high dimensional integrals. On the other hand, one of the method limitation resides in the inherent size limitation of EGO coupled with the Kriging metamodel: the dimension  $n$  of the optimization problem.

**Acknowledgements** The authors acknowledge the financial support and thank the Brazilian research funding agencies CNPq and CAPES.

## References

- Bruce Ankenman, Barry L Nelson, and Jeremy Staum. Stochastic kriging for simulation metamodeling. *Operations research*, 58(2):371–382, 2010.
- Hyo Gil Bae, Soo Hyung Park, and Jank Hyuk Kwon. Ego method for diffusing s-duct shape design. In *International Conference on Computation Fluid Dynamics*, volume 7, 2012.
- André T Beck, Ioannis A Kougiumtzoglou, and Ketson R M dos Santos. Optimal performance-based design of non-linear stochastic dynamical rc structures subject to stationary wind excitation. *Engineering Structures*, 78:145–153, 2014.
- J. Beck, B. M. Dia, L. F. R. Espath, Q. Long, and R. Tempone. Fast Bayesian experimental design: Laplace-based importance sampling for the expected information gain. *Computer Methods in Applied Mechanics and Engineering*, 334: 523–553, June 2018. doi: 10.1016/j.cma.2018.01.053.
- Sarah Bobby, Seymour M. J. Spence, and Ahsan Kareem. Data-driven performance-based topology optimization of uncertain wind-excited tall buildings. *Structural and Multidisciplinary Optimization*, 54(6):1379–1402, Dec 2016. doi: 10.1007/s00158-016-1474-6.
- E. Capiez-Lernout and C. Soize. Robust design optimization in computational mechanics. *Journal of Applied Mechanics, Transactions ASME*, 75(2):021001–1–021001–11, 2008.
- Subrata Chakraborty and Bijan Kumar Roy. Reliability based optimum design of tuned mass damper in seismic vibration control of structures with bounded uncertain parameters. *Probabilistic Engineering Mechanics*, 26(2):215–221, 2011.
- Anirban Chaudhuri, Raphael T. Haftka, Peter Ifju, Kelvin Chang, Christopher Tyler, and Tony Schmitz. Experimental flapping wing optimization and uncertainty quantification using limited samples. *Structural and Multidisciplinary Optimization*, 51(4):957–970, Apr 2015. ISSN 1615-1488. doi: 10.1007/s00158-014-1184-x.
- W F Chen and E M Lui. *Handbook of Structural Engineering, Second Edition*. CRC Press, Boca Raton, FL, USA, 2005. ISBN 9781420039931.
- Xi Chen and Kyoung-Kuk Kim. Stochastic kriging with biased sample estimates. *ACM Transactions on Modeling and Computer Simulation (TOMACS)*, 24(2):8, 2014.
- Xi Chen, Bruce E Ankenman, and Barry L Nelson. The effects of common random numbers on stochastic kriging metamodels. *ACM Transactions on Modeling and Computer Simulation (TOMACS)*, 22(2):7, 2012.
- Xi Chen, Bruce E Ankenman, and Barry L Nelson. Enhancing stochastic kriging metamodels with gradient estimators. *Operations Research*, 61(2):512–528, 2013.
- Ivo Couckuyt, Frederick Declercq, Tom Dhaene, Hendrik Rogier, and Luc Knockaert. Surrogate-based infill optimization applied to electromagnetic problems. *International Journal of RF and Microwave Computer-Aided Engineering*, 20(5): 492–501, 2010.
- Noel Cressie. *Statistics for spatial data*, volume 15. Wiley, New York, 1993.
- Richard O Duda, Peter E Hart, and David G Stork. *Pattern classification*. John Wiley & Sons, 2012.
- Régis Duvinéau and Praveen Chandrashekar. Kriging-based optimization applied to flow control. *International Journal for Numerical Methods in Fluids*, 69(11):1701–1714, 2012.
- Miguel Letícia Fleck Fadel, Miguel Leandro Fleck Fadel, and Lopez Rafael Holdorf. Failure probability minimization of buildings through passive friction dampers. *The Structural Design of Tall and Special Buildings*, 25(17):869–885, 2016.
- Alexander Forrester, Andras Sobester, and Andy Keane. *Engineering design via surrogate modelling: a practical guide*. John Wiley & Sons, Chichester, West Sussex, United Kingdom, 2008.
- E Gengembre, Bruno Ladevie, Olivier Fudym, and A Thuillier. A kriging constrained efficient global optimization approach applied to low-energy building design problems. *Inverse Problems in Science and Engineering*, 20(7):1101–1114, 2012.
- Michael B Giles. Multilevel monte carlo path simulation. *Operations Research*, 56(3):607–617, 2008.

- Tushar Goel, Raphael T. Haftka, and Wei Shyy. Comparing error estimation measures for polynomial and kriging approximation of noise-free functions. *Structural and Multidisciplinary Optimization*, 38(5):429, Aug 2008. ISSN 1615-1488. doi: 10.1007/s00158-008-0290-z.
- Wellison J.S. Gomes, André T. Beck, Rafael H. Lopez, and Leandro F.F. Miguel. A probabilistic metric for comparing metaheuristic optimization algorithms. *Structural Safety*, 70: 59 – 70, 2018. ISSN 0167-4730.
- RB Gramacy and HKH Lee. Optimization under unknown constraints. In *Proceedings of the sixth Valencia international meeting*, USA, 2010. Oxford University Press.
- Raphael T. Haftka, Diane Villanueva, and Anirban Chaudhuri. Parallel surrogate-assisted global optimization with expensive functions – a survey. *Structural and Multidisciplinary Optimization*, 54(1):3–13, Jul 2016. ISSN 1615-1488. doi: 10.1007/s00158-016-1432-3.
- Abdul-Lateef Haji-Ali, Fabio Nobile, and Raúl Tempone. Multi-index monte carlo: when sparsity meets sampling. *Numerische Mathematik*, 132(4):767–806, 2016.
- John Michael Hammersley and David Christopher Handscomb. General principles of the monte carlo method. In *Monte Carlo Methods*, pages 50–75. Springer, 1964.
- Peng Hao, Shaojun Feng, Ke Zhang, Zheng Li, Bo Wang, and Gang Li. Adaptive gradient-enhanced kriging model for variable-stiffness composite panels using isogeometric analysis. *Structural and Multidisciplinary Optimization*, pages 1–16, 2018. doi: 10.1007/s00158-018-1988-1.
- Xun Huan and Youssef M Marzouk. Simulation-based optimal bayesian experimental design for nonlinear systems. *Journal of Computational Physics*, 232(1):288–317, 2013.
- Deng Huang, Theodore T Allen, William I Notz, and Ning Zeng. Global optimization of stochastic black-box systems via sequential kriging meta-models. *Journal of global optimization*, 34(3):441–466, 2006.
- Zhangjun Huang, Chengen Wang, Jian Chen, and Hong Tian. Optimal design of aeroengine turbine disc based on kriging surrogate models. *Computers & structures*, 89(1):27–37, 2011.
- Alexander I J. Forrester, Andy J Keane, and Neil W Bressloff. Design and analysis of "noisy" computer experiments. *AIAA journal*, 44(10):2331–2339, 2006.
- Hamed Jalali, Inneke Van Nieuwenhuysse, and Victor Picheny. Comparison of kriging-based algorithms for simulation optimization with heterogeneous noise. *European Journal of Operational Research*, 261(1):279 – 301, 2017. ISSN 0377-2217. doi: <https://doi.org/10.1016/j.ejor.2017.01.035>.
- Donald Jones. A Taxonomy of Global Optimization Methods Based on Response Surfaces. *Journal of Global Optimization*, 21(4):345–383, 2001. doi: 10.1023/a:1012771025575.
- Donald R Jones, Matthias Schonlau, and J William. Efficient Global Optimization of Expensive Black-Box Functions. *Journal of Global Optimization*, 13:455–492, 1998. ISSN 09255001. doi: 10.1023/a:1008306431147.
- M.H. Kalos and P.A. Whitlock. *Monte Carlo Methods, Volume 1: Basics*. Monte Carlo Methods. Wiley, 1986. ISBN 9780471898399.
- Bogumił Kamiński. A method for the updating of stochastic kriging metamodels. *European Journal of Operational Research*, 247(3):859–866, 2015.
- Kiyoshi Kanai. Semi-empirical formula for the seismic characteristics of the ground. 35, 07 1957.
- Masahiro Kanazaki, T Matsumo, Kengo Maeda, and Mitsuhiro Kawazoe. Efficient global optimization applied to multi-objective design optimization of lift creating cylinder using plasma actuators. In *Proceedings of the 18th Asia Pacific symposium on intelligent and evolutionary systems*, volume 1, pages 663–677, 2015.
- Jack P C Kleijnen and Ehsan Mehdad. Estimating the variance of the predictor in stochastic kriging. *Simulation Modelling Practice and Theory*, 66:166–173, 2016.
- Daniel G. Krige. A Statistical Approach to Some Basic Mine Valuation Problems on the Witwatersrand. *Journal of the Chemical, Metallurgical and Mining Society of South Africa*, 52(6):119–139, December 1951. doi: 10.2307/3006914.
- Rodolphe Le Riche and Raphael T. Haftka. On global optimization articles in smo. *Structural and Multidisciplinary Optimization*, 46(5):627–629, Nov 2012. ISSN 1615-1488. doi: 10.1007/s00158-012-0785-5. URL <https://doi.org/10.1007/s00158-012-0785-5>.
- Jin Li and Andrew D Heap. A review of comparative studies of spatial interpolation methods in environmental sciences: performance and impact factors. *Ecological Informatics*, 6(3-4):228–241, 2011.
- M. Locatelli. Bayesian algorithms for one-dimensional global optimization. *Journal of Global Optimization*, 10(1):57–76, 1997. ISSN 1573-2916. doi: 10.1023/A:1008294716304.
- Rafael H. Lopez, Leandro F. F. Miguel, and André T. Beck. *Tuned Mass Dampers for Passive Control of Structures Under Earthquake Excitations*, pages 3814–3823. Springer Berlin Heidelberg, Berlin, Heidelberg, 2015. ISBN 978-3-642-35344-4. doi: 10.1007/978-3-642-35344-4\_215.
- R.H. Lopez, T.G. Ritto, Rubens Sampaio, and J.E. Souza de Cursi. A new algorithm for the robust optimization of rotor-bearing systems. *Engineering Optimization*, 46(8): 1123–1138, 2014. doi: 10.1080/0305215X.2013.819095.
- M.A. Luersen, R. Le Riche, and F. Guyon. A constrained, globalized, and bounded nelder–mead method for engineering optimization. *Structural and Multidisciplinary Optimization*, 27(1):43–54, May 2004.
- Marco A Luersen and Rodolphe Le Riche. Globalized nelder–mead method for engineering optimization. *Computers & structures*, 82(23):2251–2260, 2004.
- Giancarlo Zibetti Mantovani, Leandro Fleck Fadel Miguel, Rafael Holdorf Lopez, Leticia Fleck Fadel Miguel, and Andre J Torii. Optimum design of multiple friction tuned mass dampers under seismic excitations. *Proceedings of the 6th international symposium on solid mechanics*, Joinville, pages 521–535, 2017.
- MATLAB version 8.6.0.267246 (R2015b)*. The Mathworks, Inc., Natick, Massachusetts, 2015.
- R. E. Melchers and A. T. Beck. *Structural Reliability Analysis and Prediction*. John Wiley & Sons, 2018.
- Leandro F.F. Miguel, Rafael H. Lopez, André J. Torii, Leticia F.F. Miguel, and André T. Beck. Robust design optimization of tmds in vehicle–bridge coupled vibration problems. *Engineering Structures*, 126:703 – 711, 2016. ISSN 0141-0296.
- Leandro Fleck Fadel Miguel, Rafael Holdorf Lopez, and Leticia Fleck Fadel Miguel. A hybrid approach for damage detection of structures under operational conditions. *Journal of Sound and Vibration*, 332(18):4241 – 4260, 2013. ISSN 0022-460X.
- Mohtasham Mohebbi, Kazem Shakeri, Yavar Ghanbarpour, and Hossein Majzoub. Designing optimal multiple tuned mass dampers using genetic algorithms (GAs) for mitigating the seismic response of structures. *Journal of Vibration and Control*, 19(4):605–625, 2013.
- Douglas C Montgomery and George C Runger. *Applied statistics and probability for engineers*. John Wiley & Sons, New York, USA, 2010.
- John A Nelder and Roger Mead. A simplex method for function minimization. *The computer journal*, 7(4):308–313, 1965.

- Idilson Antônio Nhamage, Rafael Holdorf Lopez, and Leandro Fleck Fadel Miguel. An improved hybrid optimization algorithm for vibration based-damage detection. *Advances in Engineering Software*, 93:47 – 64, 2016. ISSN 0965-9978. doi: <https://doi.org/10.1016/j.advengsoft.2015.12.003>.
- Michael A Osborne, Roman Garnett, and Stephen J Roberts. Gaussian processes for global optimization. In *3rd international conference on learning and intelligent optimization (LION3)*, pages 1–15, 2009.
- Victor Picheny and David Ginsbourger. Noisy kriging-based optimization methods: a unified implementation within the diceoptim package. *Computational Statistics & Data Analysis*, 71:1035–1053, 2014.
- Victor Picheny, David Ginsbourger, Yann Richet, and Gregory Caplin. Quantile-based optimization of noisy computer experiments with tunable precision. *Technometrics*, 55(1):2–13, 2013a.
- Victor Picheny, Tobias Wagner, and David Ginsbourger. A benchmark of kriging-based infill criteria for noisy optimization. *Structural and Multidisciplinary Optimization*, 48(3): 607–626, 2013b.
- Matthew Plumlee and Rui Tuo. Building accurate emulators for stochastic simulations via quantile kriging. *Technometrics*, 56(4):466–473, 2014.
- Huashuai Qu and Michael C Fu. Gradient extrapolated stochastic kriging. *ACM Transactions on Modeling and Computer Simulation (TOMACS)*, 24(4):23, 2014.
- T. G. Ritto, R. H. Lopez, R. Sampaio, and J. E. Souza De Cursi. Robust optimization of a flexible rotor-bearing system using the campbell diagram. *Engineering Optimization*, 43(1):77–96, 2011.
- R. Y. Rubinstein. *Simulation and the Monte Carlo Method*. John Wiley & Sons, 2007.
- Jerome Sacks, William J. Welch, Toby J. Mitchell, and Henry P. Wynn. Design and analysis of computer experiments. *Statist. Sci.*, 4(4):409–423, 11 1989. doi: 10.1214/ss/1177012413.
- Sei-ichiro Sakata, Fumihiro Ashida, and Hiroyoshi Tanaka. Kriging-based convex subspace single linkage method with path-based clustering technique for approximation-based global optimization. *Structural and Multidisciplinary Optimization*, 44(3):393–408, Sep 2011. ISSN 1615-1488. doi: 10.1007/s00158-011-0643-x.
- Warren Scott, Peter Frazier, and Warren Powell. The correlated knowledge gradient for simulation optimization of continuous parameters using gaussian process regression. *SIAM Journal on Optimization*, 21(3):996–1026, 2011.
- Haihui Shen, L Jeff Hong, and Xiaowei Zhang. Enhancing stochastic kriging for queueing simulation with stylized models. *IIEE Transactions*, (just-accepted), 2018.
- C. Soize, E. Capiez-Lernout, and R. Ohayon. Robust updating of uncertain computational models using experimental modal analysis. *Mechanical Systems and Signal Processing*, 22(8): 1774–1792, 2008.
- Seymour M J Spence and Ahsan Kareem. Performance-based design and optimization of uncertain wind-excited dynamic building systems. *Engineering Structures*, 78:133–144, 2014.
- Jeremy Staum. Better simulation metamodeling: The why, what, and how of stochastic kriging. In *Proceedings of the 2009 Winter Simulation Conference (WSC)*, pages 119–133, Austin, TX, USA, 2009. IEEE.
- Hiroshi Tajimi. A statistical method of determining the maximum response of a building structure during an earthquake. In *Proceedings of the 2nd World Conference on Earthquake Engineering*, pages 781–797, Tokyo, Japan, 1960.
- Nicolaos Theodossiou and Pericles Latinopoulos. Evaluation and optimisation of groundwater observation networks using the kriging methodology. *Environmental Modelling & Software*, 21(7):991–1000, 2006.
- André Jacomet Torii, Rafael Holdorf Lopez, and Marco Antônio Luersen. A local-restart coupled strategy for simultaneous sizing and geometry truss optimization. *Latin American Journal of Solids and Structures*, 8:335 – 349, 09 2011. ISSN 1679-7825. doi: 10.1590/S1679-78252011000300008.
- Selvakumar Ulaganathan, Ivo Couckuyt, Tom Dhaene, Eric Laermans, and Joris Degroote. On the use of gradients in kriging surrogate models. In *Simulation Conference (WSC), 2014 Winter*, pages 2692–2701. IEEE, 2014.
- Samee Ur Rehman and Matthijs Langelaar. Adaptive efficient global optimization of systems with independent components. *Structural and Multidisciplinary Optimization*, 55(4):1143–1157, Apr 2017. ISSN 1615-1488. doi: 10.1007/s00158-017-1663-y.
- Emmanuel Vazquez, Julien Villemonteix, Maryan Sidorkiewicz, and Eric Walter. Global optimization based on noisy evaluations: an empirical study of two statistical approaches. In *Journal of Physics: Conference Series*, volume 135, page 012100. IOP Publishing, 2008.
- Julien Villemonteix, Emmanuel Vazquez, and Eric Walter. An informational approach to the global optimization of expensive-to-evaluate functions. *Journal of Global Optimization*, 44(4):509, 2009.
- Kai Wang, Xi Chen, Feng Yang, Dale W Porter, and Nianqiang Wu. A new stochastic kriging method for modeling multi-source exposure-response data in toxicology studies. *ACS sustainable chemistry & engineering*, 2(7):1581–1591, 2014.
- Qiong Zhang and Wei Xie. Asymmetric kriging emulator for stochastic simulation. In *Proceedings of the 2017 Winter Simulation Conference*, page 137. IEEE Press, 2017.
- Ping Zhu, L W Zhang, and K M Liew. Geometrically nonlinear thermomechanical analysis of moderately thick functionally graded plates using a local petrov-galerkin approach with moving kriging interpolation. *Composite Structures*, 107: 298–314, 2014.
- L. Zou and X. Zhang. Stochastic Kriging for Inadequate Simulation Models. *ArXiv e-prints*, February 2018.

## Appendix A Deterministic Kriging

Deterministic Kriging constructs a prediction model  $\hat{y}$  based on the available information of the current sampling plan -  $\mathbf{I}$  and  $\mathbf{y}$  - using Kriging (Sacks et al., 1989). The basic idea behind Kriging is to construct a metamodel whose response at any point  $\mathbf{d}$  is modeled as a realization of a stationary stochastic process. Thus, at any point on the design domain, we have a Normal random variable with mean  $\mu$  and variance  $\sigma^2$ . Considering an initial sampling plan  $\mathbf{I}$ , the covariance between any two input points  $\mathbf{d}^{(i)}$  and  $\mathbf{d}^{(j)}$  is:

$$\text{Cov}[\mathbf{d}^{(i)}, \mathbf{d}^{(j)}] = \sigma^2 \Psi(\mathbf{d}^{(i)}, \mathbf{d}^{(j)}), \quad (38)$$

where  $\Psi$  is the correlation matrix, which has the form:

$$\Psi(\mathbf{d}^{(i)}, \mathbf{d}^{(j)}) = \sum_{k=1}^n \exp\left(-\theta_k \left|d_k^{(i)} - d_k^{(j)}\right|^{p_k}\right). \quad (39)$$

The unknown parameters  $\theta_k$  and  $p_k$  may be found by Maximum Likelihood Estimate (MLE) (Montgomery and Runger,

2010), which then gives us the mean value - or average trend - and variance of the approximation:

$$\hat{\boldsymbol{\mu}} = \frac{\mathbf{1}^T \boldsymbol{\Psi}^{-1} \mathbf{y}}{\mathbf{1}^T \boldsymbol{\Psi}^{-1} \mathbf{1}} \quad (40)$$

and

$$\hat{\sigma}^2 = \frac{(\mathbf{y} - \mathbf{1}\hat{\boldsymbol{\mu}})^T \boldsymbol{\Psi}^{-1} (\mathbf{y} - \mathbf{1}\hat{\boldsymbol{\mu}})}{n_s}, \quad (41)$$

where  $\mathbf{1}$  is the identity matrix. With the estimated parameters, the Kriging prediction at a given point  $\mathbf{d}_u$  is:

$$\hat{y}(\mathbf{d}_u) = \underbrace{\hat{\boldsymbol{\mu}}}_{\text{Trend}} + \underbrace{\mathbf{r}^T \boldsymbol{\Psi}^{-1} (\mathbf{y} - \mathbf{1}\hat{\boldsymbol{\mu}})}_{\text{Model uncertainty}}, \quad (42)$$

where  $\mathbf{r}$  is the vector of correlations of  $\mathbf{d}_u$  with the other  $n_s$  Kriging sampled points. The second term in the right-hand-side of Eq. (42) may be viewed as the model uncertainty since its value is inferred based on the function value of the points of the sampling plan.

One of the key benefits of kriging and other Gaussian process based models is the provision of an estimated error in its predictions. The Mean Squared Error (MSE), derived by Sacks et al. (1989) using the standard stochastic process approach reads:

$$s^2(\mathbf{d}) = \hat{\sigma}^2 \left[ 1 - \mathbf{r}^T \boldsymbol{\Psi}^{-1} \mathbf{r} + \frac{(1 - \mathbf{1}^T \boldsymbol{\Psi}^{-1} \mathbf{r})^2}{\mathbf{1}^T \boldsymbol{\Psi}^{-1} \mathbf{1}} \right]. \quad (43)$$

Eq. (43) has the intuitive property that it is zero at already sampled points. In other words, the deterministic case of Kriging acts as a regression model which exactly interpolates the observed input/output data, *i.e.*  $\hat{y}(\mathbf{d}^{(i)}) = y^{(i)}$ .

Hence, deterministic Kriging assumes that the original model always provides an exact response, *i.e.*  $y^{(i)} = J(\mathbf{d}^{(i)})$ . In other words, there is no error or variability when the original function  $J$  is evaluated. However, it is not the case analyzed in this paper. Recall that we assume that Eq. (1) may not be analytically evaluated and we want to approximate it using MCI. Thus, for a given design vector  $\mathbf{d}$ , Eq. (2) gives the approximation of the integral and Eq. (3) estimates the variance of the error in such an approximation. Consequently, when MCI is employed for the computation of  $J$ , the assumption made by deterministic Kriging no longer holds. Our goal is then to take this variability into account by constructing the metamodel using SK and including the information given by Eq. (3) into the metamodel framework.

## Appendix B Time-dependent reliability of oscillators

This section briefly presents the out-crossing approach for time dependent reliability problems. For a more detailed description, the reader is referred to Melchers and Beck (2018). The time-variant reliability problem for the random system response displacement can be formulated as follows. During a zero mean excitation event of specified duration  $t_E$ , the response of the oscillator should not exceed the specified limit - or barrier -  $\pm b$ . The barrier  $b$  in this paper is the maxim displacement of top floor. If we have knowledge of system response statistics

we may evaluate the out-crossing rate of the system, and consequently, its probability of failure. For a linear system excited by a zero mean Gaussian process, the response is Gaussian and the up-crossing rate can be evaluated as

$$v_z^+(\mathbf{d}, \mathbf{X}) = \frac{\sigma_{\dot{z}}(\mathbf{d}, \mathbf{X})}{\sigma_z(\mathbf{d}, \mathbf{X})} \frac{1}{2\pi} \exp\left(-\frac{b^2}{2(\sigma_z(\mathbf{d}, \mathbf{X}))^2}\right), \quad (44)$$

where  $\sigma_z$  and  $\sigma_{\dot{z}}$  are the standard deviation of the displacement and of the velocity response, respectively. In Eq. (44), we make explicit the dependence of the crossing rate on the design variables  $\mathbf{d}$  as well as the random parameters  $\mathbf{X}$  of the problem. Thus, considering a stationary excitation, the probability of a failure event  $F$  of a given duration  $t_E$  may be computed as

$$P(F|\mathbf{d}, \mathbf{X}, t_E) = 1 - \exp\left(-2 \int_0^{t_E} v_z^+(\mathbf{d}, \mathbf{X}) dt\right), \quad (45)$$

$$= 1 - \exp(-2t_E v_z^+(\mathbf{d}, \mathbf{X})). \quad (46)$$

$$(47)$$

The structural loading from an earthquake, which is the application topic, is described by the arrival of an unknown number of events. Hence, the arrival of the events is modeled here as a Poisson process. Thus, for a design life  $t_D$  with a number of events  $n_e$ , we define the probability of failure  $P_f$  as

$$P_f(\mathbf{d}, \mathbf{X}) := P(F|\mathbf{d}, \mathbf{X}, t_D), \quad (48)$$

$$= \sum_{i=1}^{\infty} P(F|\mathbf{d}, \mathbf{X}, t_E, n_e = i) P(n_e = i|t_D), \quad (49)$$

where

$$P(F|\mathbf{d}, \mathbf{X}, t_E, n_e = i) = 1 - (1 - P(F|\mathbf{d}, \mathbf{X}, t_E))^i \quad (50)$$

$$P(n_e = i|t_D) = \frac{(\nu t_D)^i \exp(-\nu t_D)}{i!}, \quad (51)$$

in which  $\nu$  is the arrival rate of events. We may now obtain the reliability index  $\beta$  from the  $P_f$  given in Eq. (48) as

$$\beta(\mathbf{d}, \mathbf{X}) := -\Phi^{-1}(P_f(\mathbf{d}, \mathbf{X})), \quad (52)$$

where  $\Phi$  is the standard Gaussian cumulative distribution function.

Note that the reliability index in Eq. (52) still depends on the random vector  $\mathbf{X}$ , characterized by its joint probability density function  $f_{\mathbf{X}}$ . Consequently, in order to compute the resulting structural reliability, we must then employ the Total Probability Theorem, leading to

$$\bar{\beta}(\mathbf{d}) := \mathbb{E}_{\mathbf{X}}[\beta(\mathbf{d}, \mathbf{X})] \quad (53)$$

$$= \int_{\mathbf{X}} \beta(\mathbf{d}, \mathbf{x}) f_{\mathbf{X}}(\mathbf{x}) d\mathbf{x} \quad (54)$$

where  $\mathbb{E}$  is the expected value operator and  $\bar{\beta}(\mathbf{d})$  is the objective function to be maximized in the optimization process.



## Appendix C Globalized Bounded Nelder–Mead (GBNM)

The Globalized Bounded Nelder–Mead method employs a local search with a probabilistic restart, where the restart procedure uses an adaptive probability density function constructed using the memory of past local searches, as per Luersen and Le Riche (2004). The resulting optimization algorithm (coupling of the aforementioned restart and different local optimization algorithms) has been successfully applied to solve structural optimization problems (Luersen and Le Riche (2004), Ritto et al. (2011), Torii et al. (2011)) and it is described in the sequel.

In this paper, the local search employed was the same as in Luersen and Le Riche (2004), namely, Bounded Nelder–Mead. A starting point  $\mathbf{s}_0$  is chosen, then, a local search is performed and when a local minimum is found, the search is restarted. This restart procedure is described below.

The probability of having sampled a point  $\mathbf{s}$  is described by a Gaussian-Parzen-window approach Duda et al. (2012):

$$f(\mathbf{s}) = \frac{1}{M} \sum_{i=1}^M f_i(\mathbf{s}), \quad (55)$$

where  $M$  is the number of points  $\mathbf{s}_{(i)}$  already sampled. Such points come from the memory kept from the previous local searches, being, in the present version of the algorithm, all the starting points and local optima already found.  $f_i(\mathbf{s})$  is the Normal multivariate probability density function given by:

$$f_i(\mathbf{s}) = \frac{1}{(2\pi)^{n_p/2} \det([\Sigma])^{1/2}} \exp\left(-\frac{1}{2}(\mathbf{s} - \mathbf{s}_{(i)})^T [\Sigma]^{-1} (\mathbf{s} - \mathbf{s}_{(i)})\right), \quad (56)$$

where  $n_p$  is the problem dimension and  $[\Sigma]$  is the covariance matrix:

$$[\Sigma] = \begin{bmatrix} \sigma_1^2 & & \\ & \ddots & \\ & & \sigma_{n_p}^2 \end{bmatrix}. \quad (57)$$

The variances are estimated by the relation:

$$\sigma_j^2 = \beta_o (s_j^{\max} - s_j^{\min})^2 \quad (58)$$

where  $\beta_o$  is a positive parameter that controls the length of the Gaussians, and  $s_j^{\max}$  and  $s_j^{\min}$  are the bounds of the  $j^{th}$  variable ( $j = 1, 2, \dots, n_p$ ). To keep the method simple, such variances are kept constant during the optimization process. At the end of each local search,  $N$  points are randomly sampled ( $\mathbf{s}_1, \mathbf{s}_2, \dots, \mathbf{s}_N$ ) and the one that minimizes Eq.(55) is selected as the initial point to restart the next local search. The stopping criterion of the global optimization of each subproblem is the maximum number of restarts ( $nr_{max}$ ) defined *a priori* by the user.